Title
VALIDATION STUDY OF VORTEX METHODS

Authors
Sethian, J.A.
Ghoneim, A.F.

Publication Date
1986-05-01

Lawrence Berkeley Laboratory
UNIVERSITY OF CALIFORNIA

Physics Division

MATHEMATICS DEPARTMENT

To be submitted for publication

VALIDATION STUDY OF VORTEX METHODS

J.A. Sethian and A.F. Ghoneim

May 1986

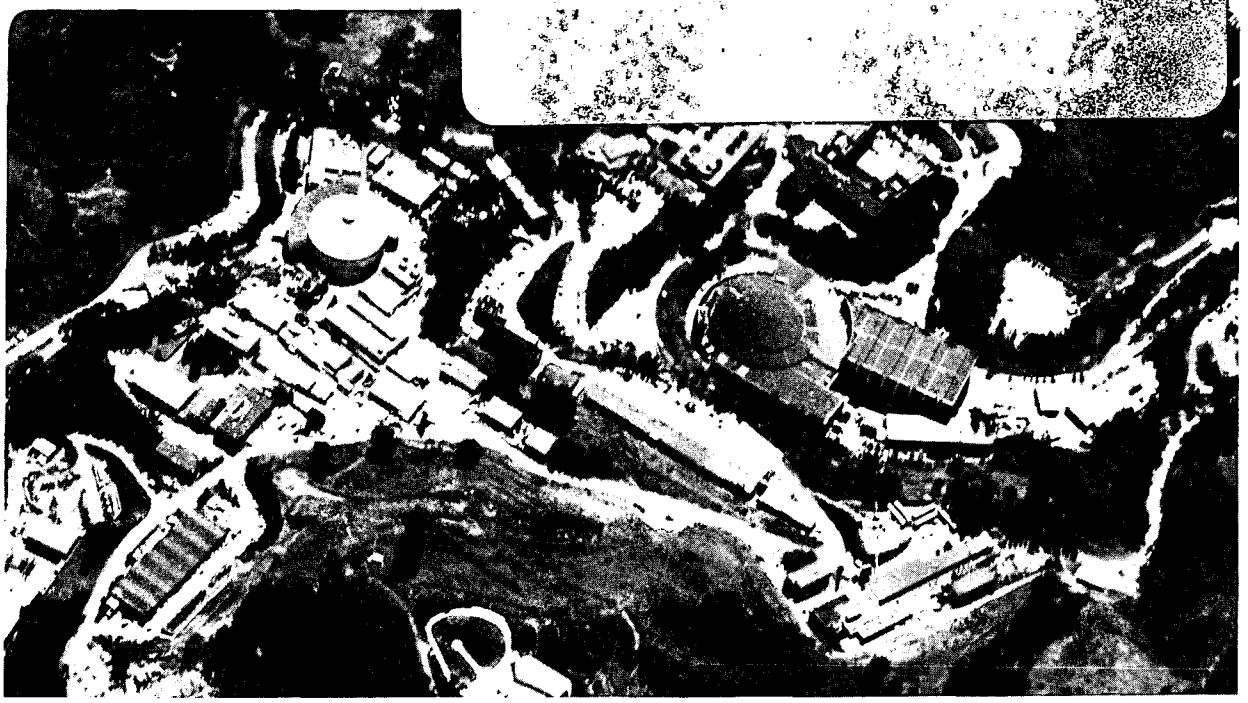

Prepared for the U.S. Department of Energy under Contract DE-AC03-76SF00098

DISCLAIMER

LBL-21767

VALIDATION STUDY OF VORTEX METHODS[1]

James A. Sethian

Department of Mathematics and Lawrence Berkeley Laboratory
University of California
Berkeley, California 94720

Ahmed F. Ghoneim

Department of Mechanical Engineering
Massachusetts Institute of Technology
Cambridge, Massachusetts 02139

May 1986

[1]Supported in part by the Applied Mathematical Sciences Subprogram of the Office of Energy Research, U.S. Department of Energy under contract DE-AC03-76SF00098, the National Science Foundation under the National Science Foundation Mathematical Sciences Post-Doctoral Fellowship Program, the National Science Foundation Grant CPE-8404811, and the Air Force Office of Scientific Research under Grant AFOSR84-0356.

Validation Study of Vortex Methods

James A. Sethian
Department of Mathematics
University of California, Berkeley
Berkeley, California 94720

Ahmed F. Ghoniem
Department of Mechanical Engineering
Massachusetts Institute of Technology
Cambridge, Massachusetts 02139

Convergence of the vortex method applied to viscous, incompressible flow is studied. We compute the solution of flow over a backwards-facing step for Reynolds number 50, 125, 250, 375, 500 and 5000, and study the effect of the choice of numerical parameters on the accuracy of the computed solution. Within the laminar regime, we demonstrate pointwise convergence of computed velocity fields to experimental measurements, decay of variance around the computed mean inversely proportional to the number of vortex elements, and accurate prediction of size and length of recirculation zones as a function of Reynolds number. At higher Reynolds number, we show detailed calculations of eddy shedding and pairing, and qualitative numerical convergence in such flow variables as eddy size and average velocity profiles.

Submitted to The Journal of Computational Physics

This work was supported in part by the Applied Mathematics Subprogram of the Office of Energy Research, U.S. Department of Energy under contract DE-AC03-76SF00098, the National Science Foundation under the National Science Foundation Mathematical Sciences Post-Doctoral Fellowship Program, the National Science Foundation Grant CPE-8404811, and the Air Force Office of Scientific Research under Grant AFOSR84-0356.

Validation Study of Vortex Methods

I. INTRODUCTION

In this paper we present a careful and detailed convergence study of the vortex method applied to viscous, incompressible, two-dimensional flow. We compute the solution to flow over a backwards-facing step over a wide range of Reynolds numbers, from laminar through transitional to turbulent flow. The effect of the choice of time step, number of particles, boundary layer resolution, core size and domain truncation length is analyzed by comparing the converged computed solution to experimental measurements. From this study emerges a healthy and heartening portrait of the method: pointwise convergence of computed velocity fields to experimental measurements in the laminar regime, decay of variance inversely proportional to the number of vortex elements, accurate prediction of size and length of recirculating zones as a function of Reynolds number, detailed and successful calculations of eddy shedding and pairing at higher Reynolds numbers, and qualitative numerical convergence in such critical flow variables as eddy size and average velocity profiles.

The vortex method relies on a discretization of the continuous time-dependent vorticity field into a large number of interacting vortex "blobs", whose position and strengths determine the underlying velocity field. Viscous diffusion is approximated by a random walk imposed on the vortex motion, and the no-slip requirement along the boundary is satisfied by a vorticity creation algorithm. While this method has gained considerable popularity in recent years, and has been used in a variety of settings (see [4,9,10,17,18,27,30,33,35,41,42,43,44]), the surprising effectiveness, reliability and accuracy of the algorithm was not fully appreciated. Previous applications have focussed on reproducing gross qualitative structures of highly turbulent flow. Due to the unsteady nature of such flow, the usual goal has been to predict qualitative gross features such as the presence of recirculation zones and global fluid struc-

tures. These are integrated quantities however, and ideally one would like to know how the accuracy of the computed values of local instantaneous velocity, pressure, etc., depend on the choice of numerical parameters. Unfortunately, since the equations model a turbulent phenomenon, exact solutions seldom exist, and experimental measurements usually come in the form of averaged quantities. Thus, it is not straightforward to perform the standard convergence study of comparing the computed solution to the exact solution as a function of the numerical parameters.

In order to subject the algorithm to critical examination, we studied the problem of flow over a backwards-facing step, chosen because of the wealth of experimental data available under a variety of flow conditions. Within the laminar regime, the fully developed flow is stable and steady, providing a setting for pointwise convergence of computed velocity fields to experimental measurements as the numerical parameters are refined. In the transitional and turbulent regime, averaged quantities such as recirculation zone lengths and average velocity profiles can be calculated and compated with experiment. In addition, there is a periodic and regular pattern to the generation and development of coherent fluid structures which should not change under refinement of numerical parameters.

It is important to point out that we study the two-dimensional Navier-Stokes equations, and this is a significant assumption that ignores such three-dimensional effects as vortex stretching. It is legitimate to wonder what we mean by "two-dimensional turbulence", and how we may compare two-dimensional calculations with experiment. The approach taken here is that results are indeed two-dimensional at low Reynolds numbers, and analysis of the 2-D Navier-Stokes equations from low to moderate Reynolds number can provide insight into the transition from steady to unsteady flow. Thus, with respect to our calculations, the word "turbulent" shall mean the instability of small-scale flow with increasing Reynolds number and the resulting coagulation of vorticity into large fluid structures at large scales.

In practice, there are several ways to speed up the vortex method, such as fast Poisson solvers, near-field/far-field techniques, boundary layer interpolating splines, etc. In this work, we wanted to study the basic random vortex method using as few numerical parameters as possible; we refrained from using some of the more sophisticated labor-saving techniques beacuse they would have introduced even more numerical parameters. The goal was to subject the vortex method to the sort of critical examination that it must successfully pass before it can be used with full confidence. In doing so, this numerical convergence study required several thousand hours of computer time and generated massive amounts of data, enough to fill seventeen 6250 bpi tapes. Not surprisingly, we were forced to confront the related issue of developing an organized and effective way of looking at that much data, and this will be the subject of a later paper [40].

II. EQUATIONS OF MOTION

The momentum equation for two-dimensional, viscous, incompressible flow [29] is

$$\frac{D\vec{u}}{Dt} = \frac{1}{R}\nabla^2\vec{u} - \nabla P \tag{1}$$

where $\vec{u}=(u,v)$ is the velocity of the fluid, $\frac{D}{Dt}$ is the total derivative, $P=P(x,y)$ is the pressure, R is the Reynolds number ∇ is the gradient, and ∇^2 is the two-dimensional Laplacian. Taking the curl of Eqn. 1 results in the vorticity transport equation [29]

$$\partial_t \xi + (\vec{u}\cdot\nabla)\xi = (1/R)\nabla^2\xi, \tag{2}$$

where the vorticity $\xi = \nabla \mathrm{x} \vec{u}$. The flow is incompressible ($\nabla\cdot u = 0$), and on solid walls, $\vec{u} = 0$. At the openings we must supply inflow and outflow conditions.

The computational domain is divided into an interior region and a boundary layer. The two solutions are matched to produce the full flow. In the interior, the vorticity transport

equation (Eqn. 2) is split into an advection equation

$$\partial_t \xi = -(\vec{u} \cdot \nabla)\xi \tag{3}$$

with boundary condition $\vec{u} \cdot \vec{n} = 0$, where $\vec{n}$ is the unit vector normal to solid walls, and a diffusion equation

$$\partial_t \xi = (1/R)\nabla^2 \xi \,. \tag{4}$$

In the boundary layer, the Prandtl boundary layer approximation to the vorticity transport equation is used [29]. In this approximation, it is assumed that 1) vorticity is mainly produced from large variations of u in the y direction, hence $\xi = \partial v/\partial x - \partial u/\partial y \approx -\partial u/\partial y$, and 2) along the wall, diffusion of vorticity is small compared to advection, hence $\partial_x^2 \xi \approx 0$. (Here, x and y are parallel and normal to the solid wall, respectively). The vorticity advection equation becomes

$$\begin{aligned} \partial_t \xi &= -(\vec{u} \cdot \nabla)\xi \\ \partial_x u + \partial_y v &= 0 \end{aligned} \tag{5}$$

and the diffusion equation becomes

$$\partial_t \xi = \frac{1}{R} \frac{\partial^2 \xi}{\partial_y^2}. \tag{6}$$

The boundary conditions are $\vec{u} = 0$ on the wall, and $u(x, y = \infty) = U_\infty$ is prescribed. The appropriate equations in each region are shown in Figure 1.

III. THE NUMERICAL SCHEME

The basic idea behind the numerical scheme, due to Chorin [10,11], is to update ξ by following the motion of a collection of vortex elements. In the interior, smoothed out point vortices are taken (vortex blobs) as the discrete elements of vorticity; in the boundary layer, discontinuous jumps in the tangential velocity (vortex sheets) are used. Knowledge of the position of the vortex elements at any time provides the velocity field $\vec{u}$. We briefly describe the method; for details, see [42].

In the interior, the starting point is the vorticity advection equation (3). If $\vec{x}(t)$ is the position of a particle moving in the fluid at time t, then $\xi(\vec{x}(t),t) = \xi(\vec{x}(0),0)$. Imagine the initial vorticity approximated by a collection of N particles (vortex "blobs") placed on a grid of grid size h $(N = 1/h^2)$ covering the domain; each particle carries a discrete initial vorticity $\xi(\vec{x}_i(0),0)h^2$, where $\vec{x}_i(0)$ is the initial position of the particle, $1 \leq i \leq N$. Since $\nabla \cdot \vec{u} = 0$, there exists a stream function ψ such that $\vec{u} = (\psi_y, -\psi_x)$ and hence $\xi = -\nabla^2\psi$. Thus,

$$\psi(\vec{x},t) = \int G(\vec{x} - \vec{x}')\,\xi(\vec{x}',t)\,d\vec{x}' \quad , \tag{7}$$

where $G(\vec{x}-\vec{x}') = (1/(2\pi))\log|\vec{x}-\vec{x}'|$ and $\vec{x} = (x,y)$. Hence

$$\vec{u} = \int K(\vec{x} - \vec{x}')\,\xi(\vec{x}',t)\,d\vec{x}' \quad , \tag{8}$$

where $K(\vec{x} - \vec{x}') = (-y,x)/(2\pi|\vec{x} - \vec{x}'|)$. The vortex blob method replaces the singular kernel K by a smoothed kernel K_σ obtained through the convolution $K_\sigma = K * f_\sigma$, where f_σ is a smoothing function. The positions of the vortex blobs are updated from one time step to the next by numerical integration of the velocity field given in Eqn. (8). Convergence of this method was first established in [12,22]; for work relating to the theoretical aspects of this method, see [2,5,6,12,20,22,23,24,38,39]. In the calculations presented here, we use a second-order time integration scheme (Heun's method) for advecting vortex blobs, as suggested in [42].

To update the vorticity with respect to the diffusion term $R^{-1} \nabla^2 \xi$, we allow the vortex elements to undergo a random step, drawn from a Gaussian distribution with mean zero and variance $2\Delta t / R$, where Δt is the time step used in the advection scheme. Since the random walk approximates a solution to the diffusion equation, the combined motion of advection plus random step of the vortex blobs approximates the solution to the full vorticity transport equation (Eqn.2). For details, see [10].

Similarly, in the boundary layer, we update the vorticity by advection and random walk of a finite collection of vortex elements. Here, the vorticity is approximated by vortex sheets, where a vortex sheet is defined to be a line segment of length h, centered at a point (x_o, y_o) and parallel to the x axis (the wall) such that $u(x_o, y_o^+) - u(x_o, y_o^-) = -\xi$. Given a collection of vortex sheets, the velocity field can be determined from the definition of vorticity and the incompressibility relation. During one time step, vortex sheets are advanced under this advection field and allowed to undergo a random walk in the direction normal to the wall in response to the diffusion term.

The calculations in the boundary layer and interior are matched as follows: the velocity from the interior calculation parallel to the wall and a distance δ away is taken as the velocity U_∞ seen at infinity from the boundary layer. As sheets move into the interior, they become blobs and vice versa; here, the proper vorticity strength is assigned to the transformed object so that circulation is conserved.

Finally, we turn to boundary conditions. For the moment, imagine that the domain is of infinite length downstream of the step. On solid walls, we require that the velocity be zero both normal and tangential to the solid walls. The normal boundary condition may be met by finding a function ϕ such that i) $\nabla^2 \phi = 0$ and ii) $\nabla\phi \cdot \vec{n}$ exactly cancels the velocity component normal to solid walls determined by the vortex elements. Appropriate entrance and exit requirements on $\nabla\phi \cdot \vec{n}$ must also be given. Adding this potential velocity field (ϕ_x, ϕ_y) to the one obtained by the vortex elements provides a velocity field whose normal component

vanishes on solid walls.

The tangential boundary condition (no-slip condition) along solid walls is met through the creation of vortex sheets. Suppose $C_{\max}$ is the maximum circulation allowed for any one sheet. At the beginning of each time step, calculate the tangential velocity u at points spaced a distance h along the wall. If $u \neq 0$ at any point, create enough vortex sheets (where the number created depends on $C_{\max}$ to provide a transition from the no-slip condition to the value of u. This insures that the tangential boundary condition is satisfied at the beginning of each time step. Thus, the interior flow creates vorticity at the boundary due to the no-slip condition, and this vorticity is then diffused from the boundary layer into the interior.

To limit the calculations, we wish to truncate the channel at some point W_{END} downstream from the step. We do this by deleting all the vortex elements past W_{END} and ignoring the no-slip condition beyond this point. Thus, infinitely far downstream, one might imagine that the flow becomes nearly uniform (independent of x and y). In the calculation presented here, the potential function ϕ is found by a conformal transformation of the domain onto the upper half plane, see [17]: uniform flow conditions are assumed for ϕ at infinity.

IV. SETUP OF PROBLEM

Let V be a characteristic speed of the incoming flow, let W, the channel height, represent a characteristic length scale, and let ν be the kinematic viscosity of the fluid. The dimensionless Reynolds number is defined as $R = \frac{VH}{\nu}$, where H is the step height. We shall study the flow at six different values of R, namely $R = 50$, $R = 125$, $R = 250$, $R = 375$, $R = 500$, and $R = 5000$. Loosely speaking, this covers the range from viscous to early turbulent flow. We take a channel width W of two step heights H.

We give incoming boundary conditions one channel width upstream of the step along the segment $x = -1.$, $0 \leq y \leq 1$, where the origin of the coordinate system is at the lower left

corner of the channel (See Figure 2). At the entrance, we assume a uniform entrance profile $(u, v)=(1,0)$. It is important to discuss our choice of this inlet velocity profile. From the point of view of comparison with physical experiments, this entrance profile is uncommon; at low Reynolds number, a parabolic profile will develop in most experimental apparatus in the entrance section upstream of the step, To be sure, we do in fact satisfy the no-slip condition between the line $x=-1$ (channel entrance) and $x=0$ (edge of the step). Thus the flow will neither be uniform when it reaches the edge of the step, nor will it be fully-developed Poiseuille flow over such a short distance, and this will be a source of disagreement between our calculations and experiment.

There are two reasons why we chose this uniform entrance profile. Our goal here is to provide a convergence study of the vortex method; we want to focus on the effect of changing numerical parameters on the solution. First, by assuming a uniform entrance profile, all the vorticity in the flow comes from the no-slip condition along the walls, and the numerical parameters involved in the creation of vortex sheets are the sole factors in determining the total number of vortex elements (sheets and blobs). A parabolic entrance profile requires a discretization of the entrance vorticity distribution into vortex sheets and blobs; we wish to limit the manner in which vorticity is created. Second, we wish to run experiments over a wide range of Reynolds numbers. A parabolic inlet profile is dependent on the Reynolds number, and is in fact physically unstable at the high range. In the vortex method, the only manifestation of the Reynolds number is in the size of the random step taken in the solution of the diffusion equation. We want to study the eddy structure of the solution as the balance between advection and diffusion changes, always maintaining the same boundary conditions. It is important to point out however, that it is a simple matter to integrate a given inlet profile into the vortex method if desired.

The numerical parameters are linked as follows. As input, we supply the time step Δt, the sheet length h, the circulation C of an individual vortex element, and the length of the

channel downstream of the step W_{END} (see Figure 2). These parameters are connected as follows. Vortex sheets are created at points spread a distance h along the wall. Since the circulation $C = h\,\xi$, halving C doubles the number of vortex sheets; cutting h in half does not change the number of sheets created, but instead creates half as many doubly strong sheets at twice as many points. The time step Δt is a particularly intricate parameter, since it controls (a) the size of the time step used in the time integration of the advection equation, (b) the size of the random steps, (c) the size of the boundary layer δ, and (d) how often the no-slip condition is satisfied. In addition, the scaling σ of the smoothing function f is related to h by $\sigma = h/\pi$ (see [22,42]); thus the "singularity" of an individual vortex blob is controlled by the discretization of vorticity along the wall. We will not change the smoothing function itself, and shall use the smoothed structure given in [10], resulting in a stream function for a single vortex blob of strength k of

$$\psi(r) = \begin{cases} (-k/(2\pi))\log(r) & r \geq \sigma \\ (-k/(2\pi))\left((r)/\sigma + \log(r) - 1\right) & r < \sigma \end{cases} \tag{9}$$

V. COMPARISON OF CALCULATED RESULTS WITH EXPERIMENT

In this section we compare the results of our calculations with available experimental data. There are a large number of ways to define the Reynolds number $R = VL/\nu$: some choices for L have been the step height, the channel height, inlet height, and the hydraulic diameter; for the characteristic speed, investigators have used the maximum inlet velocity, the average inlet velocity assuming a parabolic profile, and the speed at which the apparatus is towed through the fluid. To compare the various experiments with our results, we instead use the classification given in [3] of the three ranges of separated flow: 1) laminar flow, in

which the flow is laminar from the separation off the step all the way beyond reattachment, 2) transitional flow, which is laminar at the separation point but becomes turbulent prior to reattachment and 3) turbulent flow, in which the boundary layer is turbulent prior to separation. We shall use the following coordinate system in our discussion: the x axis is the downstream direction, the channel height is measured along the y axis, and the spanwise direction is the z axis. Planes x =constant are essentially normal to the flow and planes z =constant are essentially parallel to the flow.

A1. Laminar Flow-Experimental Results

In the laminar regime, the flow structure is characterized by a single, elliptically shaped recirculation zone [3,13,19,25,32,37]. The flow is essentially two-dimensional; Armaly et. al. [3] found a 1% variation in the downstream velocity in the spanwise direction, and Denham and Patrick [13] found a less than 2% variation in the total flow rate in the x direction along the center plane, indicating that the flow was self-contained along that plane.

The flow is reasonably stable and steady. Kueny and Binder [28] report that velocity at a fixed grid point did not vary by more than 1% in their experimental apparatus designed for viscous/laminar flow. At the low and medium Reynolds numbers within the laminar regime, Denham and Patrick [13] report that if the apparatus is tapped, velocities within the main flow return to original values, while velocities near the reattachment point settle to new values less than 1% of the average channel velocity; this "indicates that a small range of semi-stable recirculation zone configurations exist at each Reynolds number". This is an important point, since we are using a probabilistic technique to compute the solution to a problem that evidently contains a range of stable solutions. (Note that some numerical schemes for viscous flow over a backwards step assume the solution is time-independent [3,8,21,32,37] and compute the solution by iteration). At higher Reynolds number, still within the laminar regime, time-dependent fluctuations in the reattachment point appear, with the most pronounced velocity field fluctuations occurring in the middle of the channel with

variation on the order of 5% and periods of several minutes. Denham and Patrick [13] view this as an indication of the onset of the transitional flow regime. Furthermore, at these higher ranges of laminar flow, there is a tendency for flow separation along the upper wall opposite to the reattachment point. This separation is indicated by bending streamlines and inflections in velocity profiles, but no actual separation, that is, negative velocities, are reported [13].

The basic laminar flow pattern is characterized by flow separation at the step, an elliptical recirculation zone, and downstream reattachment to the bottom wall. (Honji [25] reports that this structure develops continuously from potential flow for impulsively started flow over a step without a wall). The reattachment length x_l for laminar internal flow is seen to scale with the step height H, and most investigators refer to a normalized reattachment length $x_R = x_l/H$ which increases with Reynolds number [3,13,19,25,28]. Goldstein et. al. [19] experimentally observe an approximately linear relationship between normalized reattachment length and Reynolds number; the maximum value they could achieve experimentally was 13 before the laminar quality of the flow broke down.

The center of the reattachment eddy ("normalized eddy center") remains nearly constant when normalized with respect to the reattachment length, with coordinates $(x_C, y_C)=(.3x_R, .6H)$, thus Denham and Patrick [13] conclude that laminar flow is essentially self-similar in that experimental values for the normalized reattachment length for different Reynolds numbers lie on a single curve, and the normalized eddy center remains fixed. As the transition stage is entered, this self-similarity breaks down.

In the laminar regime, the reattachment length is sensitive to the inlet profile. A long channel entrance ensures a parabolic velocity profile corresponding to Poiseuille flow at the step, and this is used as a requirement in designing some experimental apparatus, see [3,28]. Apparatus that do not yield fully-developed profiles at the step report shorter reattachment lengths [13], and numerical calculations based on parabolic inlet profiles usually predict slightly longer reattachment lengths than commonly measured [32] for a more uniform inlet

profile. At the exit, steady parabolic outlet profiles are reported for an 18x1 aspect ratio and low Reynolds number flow [3]; at the higher end of the laminar regime, small deviations were present.

A2. Laminar Flow-Numerical Results

We begin with the results of a calculation performed with R =50, h =.2, Δt =.05, C =.005 and W_{END}=10 (the exit section is 20 step heights downstream). In Figure 3, we show the startup from a potential flow as the no-slip condition is instantaneously imposed at t =0. We show "instantaneous streamlines" every 10 time steps: the data is not time-averaged. These streamlines are obtained as follows. A uniform grid is imposed on the domain, and the velocity at each grid point is calculated from the positions and strengths of vortex elements. Using this fixed discrete velocity field, the trajectory of a particle started within each grid cell is drawn, providing the "instantaneous streamlines". The recirculation bubble develops smoothly from the potential flow, growing in size as discussed earlier in the experimental section. In Figure 4, we show successive time portraits of the long-time behavior (the determination of when steady-state is established is discussed in the section on numerical parameters). Here, as observed experimentally, there is a single, elliptical recirculation zone with downstream reattachment to the bottom wall. The bubble is essentially steady, although definite oscillations are seen in these calculations; the variance in the computed shape depends on the number N of vortex elements, and decreases as N is increased (see section on convergence). This is a delicate point: since experimental results indicate a small range of semi-stable solutions and we are constantly perturbing the flow through our random walk solution to the diffusion equation, it is not clear that the time variation in our calculations should vanish as N goes to infinity. In any case, however, the degree of oscillation shown is probably due to the response of the solution to a high level of noise in the random walk.

A short distance downstream of the reattachment point, the flow becomes mostly parallel to the channel walls. In Figure 5, we show the streamline portrait of the flow field

averaged over 2000 time steps. The normalized reattachment length is x_R =1.7, and the calculated eddy center is at (.59,.29)=(.34x_R ,.59H), in excellent agreement with the self-similar value of (.3x_R ,.6H) reported in Denham and Patrick [13].

In Figure 6, we show successive time portraits of flow at R =125, towards the higher end of the laminar regime. We used the same numerical parameters as the calculation at R =50, thus the only difference in the two calculations is the size of the random jump in the solution of the vorticity diffusion equation, owing to the higher Reynolds number. Again, the long-time structure is an elliptical recirculation zone with essentially parallel flow a short distance downstream of the reattachment point. Small oscillations in the bubble are present. Once again, while these probably result from not using enough vortex elements, we believe that the slight unsteadiness of the real flow also plays a role here. The recirculation length from the time-averaged portrait is x_R =3.1, and the eddy center is at (1.0,.31), giving (.32x_R ,.62H), which again is in very good agreement with experiment.

B1. Transitional and Turbulent Flow-Experimental Results

The transitional stage is marked by a collapse of the two-dimensional, single recirculation eddy, stable picture of the flow. At the lower end of the transitional regime, although the flow is laminar upstream, it turns unstable over the recirculation bubble right after leaving the step [13,14]. As the Reynolds number is increased, the flow becomes three-dimensional [3], as indicated by checking spanwise velocity profiles at various points downstream, however, symmetry about the center plane is maintained. The central feature of three-dimensionality in the transition regime is the presence of longitudinal (spanwise) vortices which are responsible for dissipating structures in the flow [3]; these structures are most pronounced in the middle of the transition range, and drop out and disappear as the flow becomes turbulent.

Rather than a single steady recirculation zone, the flow is now characterized by a periodic, unsteady mechanism. Laminar flow separates from the step and becomes unsteady

midway to the reattachment point [14]. Fluid is entrained by the recirculation bubble, and eddies detach and move downstream as large eddies [3,7,13,14,19,25]. These eddies are three-dimensional in that their cross-sections vary in the spanwise direction [3]. In their study of backwards-step flow without a confining top wall, Bradshaw and Wong [7] report that the flow splits at reattachment, with the large recirculation eddy torn into two; part of the flow goes upstream into the recirculation zone to supply the entrainment and part of the eddy goes downstream, suffering a decrease in eddy length scale; similar findings were reported in [16]. In Honji's [25] study, the impulsively started flow begins as potential flow and then forms a recirculation bubble which grows, entraining more and more fluid. This bubble then "divides into three distinct vortex domains", and then sheds eddies off the downstream end of the bubble. Eddy shedding becomes more pronounced as the Reynolds number increases.

For step flow with a confining upper wall, there is a continuous mechanism of (1) fluid entrainment by a growing recirculation zone (2) detachment of eddies which move downstream resulting in (3) a smaller recirculation zone which then entrains more fluid. Within the oscillating recirculation bubble, the mean flow speed is one order of magnitude less than the mean main flow speed [26]. The large eddies move downstream and cause local flow reversal, as observed in [3,14,15,19,26]. Durst and Tropea [14] report that in the transitional regime, streamlines are wavy right after the step, and break into "vortex rolls" after 3–4 step heights downstream; as R increases, vortex formation occurs further and further upstream. Eaton and Johnson [15] characterize them as "large, turbulent, spanwise eddies" which effect large local flow reversal. These eddies are viewed as three-dimensional, responsible for dissipating structures and coupling together the various recirculation regions [3].

Transitional flow is marked by a decrease in the mean reattachment length as Reynolds number increases, in contrast with the situation in the laminar regime. The mean reattachment point is taken as the point along the bottom wall where the time averaged mean velocity field is zero; the averaging period required in order to obtain acceptably small variance of

the mean can be quite long, see [3,14,26]. Instantaneous measurements [14,26] show the reattachment point moving backwards and forwards as large eddies pass by over a distance along the bottom wall of as much as four step heights [14]; local intermittent flow reversal is observed to occur well outside this range [1,26]. The mean reattachment length decreases with increasing Reynolds number to a local minimum, at which point the shed vortices are largest [3,14].

Along the top wall, the bending streamlines found in the laminar regime now form a full new separation zone containing fluid recirculating in the opposite direction as that in the main bubble. This top wall eddy persists throughout the transition regime, and appears due to an adverse pressure gradient created by the sudden step expansion [3]. This downstream moving eddy is reported by a number of observers; time-averaged streamline plots [3,14,26] show a recirculation eddy whose position moves upstream along the top wall with increasing Reynolds number. Finally, a small, clockwise rotating recirculation eddy located at the base of the step between the corner and the large eddy has been observed by a number of researchers [3,7,28,36]; mean flow is at least two orders of magnitude slower than the main flow.

The local minimum in mean reattachment length with increasing R signals the end of the transition regime and the beginning of turbulent flow. As R increases, the mean reattachment length quickly grows to about 6–8 step heights and remains constant from then on, as reported by a large number of observers [3,14,19,26,36]: additional references are provided in [19]. Changing inlet profiles does not result in substantial change in the mean reattachment length, presumably because of the large amount of turbulence created in the separating shear layer which controls mixing and is independent of the boundary conditions, see [1]. As R increases into the turbulent regime, the size of the eddies shed off the recirculation bubble decrease in size until they finally disappear [3,14,36]. At the same time, there is an increase in turbulent mixing [14] and a return to an essentially two-dimensional flow [3].

B2. Transitional and Turbulent Flow -- Numerical Results

In Figure 7, we show the results of a calculation with R =500, well into the transitional regime, with Δt =.05, C =.025, h =.2, and W_{END}=10. The flow picture has radically changed; large eddies are shed off the recirculation bubble and progress downstream as distinct structures which decay in size, in agreement with the experiments described earlier. Once these eddies break away, calculation show that they move with very close to constant speed 1/2 V (Note that the expansion ration across the step is 1:2). This was calculated in two ways, first, by drawing a line through the center of a particular moving eddy in the successive time drawings, and second, by placing a moving time window over a given eddy and finding the reference frame speed which minimizes motion of the center. Computer-generated movies show that this "large eddy velocity" is much slower than the velocity of the particles defining its shape, analogous to the distinction between group wave velocity and individual fluid particle motion. The calculation at R =500 was carried out for 30 times longer than the time window shown (that is, 2500 time steps, counting startup), with 13 separate eddies exiting the channel during that time, an average rate of 1 eddy every 7.9 time units. In Figure 8, we stand at the point (8.0,y), which is 80% of the distance down the channel from the step, and plot the u velocity as a function of time, and height. The changes of sign in u indicating the passage of an eddy are more pronounced near the top and bottom walls (away from the middle). From this, the essentially fixed frequency of eddy shedding is seen. At this point, we do not understand why this particular frequency occurs.

In Figure 9, we show instantaneous streamline plots of a calculation for R =375 (Δt =.05, St =.025, h =.2, W_{END}=10), and, in Figure 10, for R =250, with the other parameters unchanged. At these Reynolds numbers, more towards the lower end of the transitional regime, while eddies continue to break away from the recirculation bubble, they soon dissipate at R =375 and even more quickly at R =250, due to the increase in the diffusion scale with decreasing Reynolds number. This agrees with the experimental observations

described earlier. At R =250, the eddies are almost completely diffused before they reach the exit, suggesting that the "lifetime" of the shed eddies decreases with decreasing R until the laminar, single recirculation bubble picture is reached. At both R =375 and R =250, the large eddy velocity is constant at 1/2 V, and the shedding frequency is 1 eddy every 9.8 time units at R =375 and every 9.4 time units at R =250.

Returning to the flow portrait at R =500, there are at least two ways in which our computed solution differs substantially from experimental observations. First, as discussed earlier, the real flow is three-dimensional, and shed vortices are spanwise three-dimensional structures. While we believe that our computed eddies are a legitimate aspect of the solution to the two-dimensional equations, the vorticity stretching term in the three-dimensional equations allows these structures to dissipate in the spanwise direction and our 2-D eddies persist longer than are they should.

Second, the results of the calculation (Figure 10) show a slightly different mechanism at the edge of the step than was observed experimentally. Most experiments describe a recirculation eddy that oscillates and is torn in two by the incoming flow; the shed eddy moves downstream and another eddy forms and grows by entraining more fluid as the process repeats itself. In the calculation shown, the new recirculation eddy is quite small, probably because we did not use enough vortices to adequately resolve this detailed mechanism. To address this issue, we refined the numerical parameters and used C =.01, Δt =.025, h =.2, and W_{END} =5, producing approximately 3 times as many vortices as were present in the earlier calculation. Successive time portraits of this calculation are shown in Figure 11. Here, one can get a better picture of the way that the oscillating recirculation bubble is stretched and distorted by the incoming flow, which tears away the downstream end of the bubble.

We then increased the Reynolds number, and in Figure 12 show the results of a calculation at R =5000, in the "two-dimensional turbulent" regime with Δt =.05, h =.2, C =.05 and W_{END}=10. Once again, the structure of the flow has changed dramatically. The bending

of streamlines seen earlier at about 3–4 step heights downstream has now turned into separation along the top wall, and counterrotating eddies are shed which interlace with eddies shed from the recirculation bubble.

Finally, we discuss the change in the mean reattachment length. In Figure 13, we show long time-averaged streamlines plots at R =50, R =125, R =250, R =375, R =500, and R =5000, and in Figure 14 we plot reattachment length as a function of Reynolds number for these plus a few more values. The reattachment length grows in a close to linear fashion, reaches a maximum somewhere between R =250 and R =375, and then falls back down, in agreement with the experimental data described earlier. At R =250, the eddy center is at (1.89,.31)=($.44x_R$,$.62H$), at R =375 at (1.59,.32)=($.38x_R$,$.64H$), at R =500 at (2.11,.29)=($.53x_R$,$.58H$), and at R =5000 at (1.8,.3)=($.66x_R$,$.6H$), showing the breakdown in the self-similar nature of the time-averaged flow at the higher Reynolds numbers. In the time-averaged plots for R =375, R =500 and R =5000, the counterrotating eddy in the lower left corner is seen. Finally, along the top wall at R =5000, we see the fixed position of the counterrotating separation eddy reported in [3,14,26]. The center of this eddy is at (4.1,.9), which is 8 step heights downstream, indicating that we are well into the "turbulent" regime.

VI. DEPENDENCE OF SOLUTION ON NUMERICAL PARAMETERS

A. Laminar Flow

We analyze the dependence of the computed solution at R =50 on numerical parameters. At this value of R , the fully developed real flow is essentially time-independent (steady). Our procedure is to analyze convergence under a variety of measures, starting from highly averaged and integrated statistics down to pointwise, instantaneous quantities.

We begin by studying the total circulation $\Gamma(t)$ in the computational domain $0 \leq x \leq 5.0$, $0 \leq y \leq 1$, calculated by summing the circulations of all the vortex elements at time t. In Figure 15, we plot $\Gamma(t)$ for various values of C (the other numerical parameters are held fixed). As C is decreased, the number N of vortex elements increases. The calculation runs from $t=0$ (start up) to $t=50.0$, which corresponds to 1000 time steps. As a reference, the total number of vortex elements at the end of the run is given in the figure as (A,B), where A is the number of vortex blobs and B is the total number of vortex elements (sheets plus blobs). At $t=0$, there is no vorticity in the domain. Long-time behavior has set in after about 200 time steps. Let $\bar{\Gamma}$ be the average value of $\Gamma(t)$ over time steps 200 to 1000. We observe that i)the oscillation of $\Gamma(t)$ around $\bar{\Gamma}$ and hence the deviation around the mean decreases as N increases and ii) $\bar{\Gamma}$ stays relatively fixed as N increases, showing convergence of the mean as N increases. To establish a convergence rate, in Figure 16 we plot the variance $\frac{1}{500} \sum_{n=500}^{1000} | \Gamma(n \Delta t) - \bar{\Gamma} |^2$ against the number of vortices. The graph roughly corresponds to a convergence rate of order $1/N$: doubling the number of vortex elements halves the variance in the solution.

In Figure 17a, we hold h, C and W_{END} fixed and decrease Δt by a factor of 2. The variance in $\Gamma(t)$ around $\bar{\Gamma}$ is about the same in both plots [7% for $\Delta t = .05$ and 8% for $\Delta t = .025$], and the mean $\bar{\Gamma}$ is virtually unchanged; $\bar{\Gamma}=.36$ for $\Delta t = .05$ and $\bar{\Gamma}=.31$ for $\Delta t = .025$. Note the additional number of vortex elements resulting from the smaller time step. These results indicate that, at low Reynolds number, the large jumps in positions of the vortices to approximate the diffusion equation dominate any increase in accuracy associated with better time integration along the particle trajectories. Thus, the numerical diffusion error associated with advecting the particles, (see [42]), is overshadowed by the actual physical viscosity.

In Figure 17b, we hold Δt, C, and W_{END} fixed and halve h, the sheet length. As explained earlier, this corresponds to a more accurate discretization of the newly created

vortex sheet in the x rather than y direction; in addition, it corresponds to taking a smaller core size in the smoothing function. For a flow that is essentially steady with a single reattachment point, little difference can be seen in the two plots (variance is 8.4% for h =.2, and 8.5% for h =.1, and the $\overline{\Gamma}$ is .52 for h =.2 and .56 for h =.1.

These results indicate that C is the most important parameter controlling accuracy for this range of flow. This is reasonable, since at low Reynolds number, the physical diffusion term is large and more vortex elements reduce the noise in the random walk solution to the diffusion equation. We check two other parameters: the dependence of the solution on the particular random number string chosen (the initializing seed) and the length of the truncated channel. In Figure 17c, we hold Δt , h , and C fixed and double the channel length and start with a different seed in the random jump subroutine. The variance is 3.5% ($\overline{\Gamma}$ = .61) for W_{END}=5 and 4.0% ($\overline{\Gamma}$ = .62) for W_{END}=10, indicating that results are essentially independent of starting seed and that W_{END}=5 is long enough for this calculation.

The total circulation is a global quantity of the flow. The next level of sensitivity is to analyze the velocity field. Since we are dealing with a Lagrangian method, we establish a velocity field by placing a grid on the domain and at each time step compute $\vec{u}_{i,j}^{\,n}$, where $\vec{u}_{i,j}^{\,n}$ is the velocity on a uniform rectangular grid at time step $n\,\Delta t$ at the point $i\,\Delta x$, $j\,\Delta y$, where $\Delta x = \Delta y$ =.1 , $0 \le i\,\Delta x \le W_{\mathrm{END}}$, $0 \le j\,\Delta y \le 1$. We want to investigate how the choice of numerical parameters affects the convergence of the mean and variance velocity field.

We begin by studying the possibility of time averaging as a technique for removing "noise", .i.e., time variation around the mean, in the solution. Let $\vec{u}_{i,j}^{\,n}(M)$ be the velocity field obtained by averaging $\vec{u}_{i,j}^{\,n}$ over M time steps. Let $Err\,(M)$ be defined as

$$Err\,(M) = \frac{1}{\mathrm{W(M)}} \sum_{\text{windows of length M}} \left(\frac{1}{\mathrm{I \cdot J}} \sum_{i,j} \mid \vec{u}_{i,j}^{\,n}(M) - \vec{u}_{i,j}^{\,n}(500) \mid^2 \right) \Big/ \left(\mid \vec{u}_{i,j}^{\,n\,(500)} \mid^2 \right),$$

where $W(M)$ is the number of windows of length M. In other words, $Err\,(M)$ is the average

relative L^2 error in the discrete velocity field between a time average portrait of length M steps and the time average portrait of length 500 steps (All averages start at time step n =500, thus M =500 corresponds to averaging over time steps 500 to 1000). In Figure 18, this quantity is plotted against M, the size of the sample window. Here, the average is taken over all "windows" of length M, and the norm $| \vec{u} | = (u^2+v^2)^{1/2}$. For example, for M =2, we calculate the average relative L^2 error between velocity fields obtained from averaging over 2 time steps and the velocity field obtained from an averaging window 500 time steps long. The results indicate that the more the numerical parameters are refined, the more the short-time average velocity field looks like the long-time average field: the dropoff for each curve is like $1/M$. Note once again that decreasing C has the most profound effect.

We next want to study the spatial and temporal variance of the velocity field from the computed mean. We begin by computing the spatial variance as a function of time. Let $\overline{u}_{i,j}$ be the velocity field obtained by averaging over time steps 500 to 1000. Then $Var^n = \frac{1}{I \cdot J} \sum_{i,j} | \vec{u}^n_{i,j} - \overline{u}_{i,j} |^2$ is the spatial variance at time $n \Delta t$ of the instantaneous field from the mean. We plot Var^n as a function of time in Figure 19, showing that as numerical parameters are refined, the instantaneous velocity field converges to the average velocity field. Again, changing C reduces the variance the most. To obtain a convergence rate, we define $\overline{Var}^n$, the spatial variance averaged in time, and plot $\overline{Var}^n$ against the number of vortices in Figure 20. The graph indicates that $\overline{Var}^n$ goes as roughly $1/N$, in agreement with our earlier estimate.

We now compute the temporal variation as a function of space, that is, at each grid point i,j we compute $Var_{i,j} = \frac{1}{500} \sum_{n=500}^{n=1000} | \vec{u}^n_{i,j} - \overline{u}_{i,j} |^2$. We plot $Var_{i,j}$ as a surface over the computational domain in Figure 21, showing that as the numerical parameters are refined, the temporal variance around the computed mean at each point decreases. In Figure 22, we calculate $Var_{i,j}$ against the number of vortices at a variety of points in the domain. Two

observations can be made. First, the curves are all roughly of the form $\frac{1}{N}$, and second, the further the spatial point is from the edge of the step, the smaller the variance.

Next we study the convergence of the mean velocity field itself as numerical parameters are refined. Using the 500 time step average of the most refined calculation ($\Delta t = .05$, $h = .2$, $C = .005$, $W_{\mathrm{END}} = 5$) as a base mean $\overline{u}_{i,j}(\mathrm{base})$, in Figure 23 we show surface plots of the relative difference between the mean velocity field $\overline{u}_{i,j}$ (the "steady-state" profile) for a given set of numerical parameters and $\overline{u}_{i,j}(\mathrm{base})$. Here, the graphs are normalized so that the largest value of any of the surfaces corresponds to a a height of unity. Note that the last surface plot is completely flat, showing, of course, no error between the finest calculation and itself. Here, one can see that the means tend towards a given profile.

Next, we again assume that the long-time average of the finest calculation (referred to as the base solution $\overline{u}_{i,j}(\mathrm{base})$ above) is a close approximation to the exact solution, and study the time variance of each calculated solution against this "exact" solution. Let $\vec{u}^{\,n}_{i,j}(\Delta t, h, C, W_{\mathrm{END}})$ be the solution at grid point i, j at time $n\,\Delta t$ with a particular set of numerical parameters and let $Err_{i,j}(\Delta t, h, C, W_{\mathrm{END}}) = \frac{1}{500}\sum_{n=500}^{n=1000} | \vec{u}^{\,n}_{i,j}(\Delta t, h, St, W_{\mathrm{END}}) - \overline{u}_{i,j}(\mathrm{base}) |^2$. These surfaces are plotted in Figure 24 and demonstrate convergence towards the base solution as the numerical parameters are refined. Again, resolution in the time step and the length of the vortex sheet has only small effect, and the decay rate of the variance is roughly $1/N$.

Finally, we wish to establish a single point, instantaneous measurement. In Figure 25, we plot the position of the reattachment point as a function of time for different numerical input parameters. The reattachment point is determined by starting at $(x = .1, y = .05)$ and moving in the positive x direction until the velocity changes sign. This is an extremely sensitive test for the vortex method, since the local instantaneous velocity field can change quite drastically if too few vortex elements are used to resolve the boundary layer. Note that the

top three calculations are sufficiently crude that the location of this point jumps wildly during a single time step. However, as the parameters are refined, the variation in position settles down and the reattachment point is relatively constant for the finer calculation.

To summarize, at low Reynolds number the variance is controlled primarily by C, which determines the number of vortex elements. Accuracy gained by refinement in time step is overshadowed by the error in the approximation to the diffusion equation due to the large diffusive scale of the flow. Changing the sheet length, which also controls the smoothing radius of the vortex core, is of secondary importance.

B. Transitional/Turbulent Flow

At higher Reynolds number, the flow is no longer steady, and a periodic structure is seen. In the portraits for $R \geq 250$ shown earlier, the flow is characterized by large coherent vortex eddies which detach from the separating shear layer and move downstream at a regular frequency. At this range of Reynolds numbers, the two-dimensional equations are unstable, and the instantaneous velocity at a particular point has little meaning. Energy (and eddies) at the smallest scales combine in an unpredictable manner, and it is only in the largest scales (coherent eddy structures) that one can see repeatability in a flow experiment.

The typical response to this has been to analyze unsteady flow by measuring variations in flow quantities around means. While certainly a valuable approach, there are two problems. First, in both experiments and numerical computations, a very long time-averaging window may be required to gain reliable statistics independent of the window size; this was observed in several of the experiments cited. Second, in many engineering applications, the main goal may not be to find mean flow statistics. Instead, one is often interested in how large-scale structures develop, the stresses they exert on the body, how they interact and how they affect mixing within the flow. Computed long-time averages remove much of the transitory dynamics. Thus, it is important to analyze the flow on some level between instantaneous measurements, which have little meaning, and long-time averaged statistics, which remove periodic

dynamics. With this approach in mind, our goal is to study the effect of refining numerical parameters on the computed large-scale eddy dynamics.

We performed a range of calculations at R =500, well outside the laminar regime. In order to make the computations affordable, we chose W_{END}=5. Calculations were performed for all combinations C =.05,.025,.01, Δt =.05,.025 and h =.2,.1, for a total of 12 runs, each running 500 time steps (1000 for Δt =.025) to become fully developed and then from 500 to 1000 (1000 to 2000 for Δt =.025) to provide data. In addition, an extremely long time (3000 time steps), extended channel (W_{END}=10), refined (C =.015, h =.2, Δt =.05) calculation was performed, providing a large sample set from which to perform statistics and compare with the shorter time/shorter channel runs. This data set allowed us to check that the results obtained for the other runs did not depend on the channel trunctation length or time length of the computation.

We begin by studying the change in the large-scale structure of the flow as numerical parameters are refined. In Figure 26, we show 6 successive time instantaneous streamlines of a calculation for C =.05, .025, .01, Δt =.05, h =.2. For C =.05, Fig. 26a, (N_{TOT} = total number of vortex elements at end of calculation = 593), the eddies are distinct structures which move downstream separately. For C =.025, Fig.26b (N_{TOT}=865), the same general picture is presented, with smoother contours around the eddies. In the case C =.05, a typical downstream eddy consists of roughly 120 vortices, as compared with 210 for C =.025. In addition, the structures for C =.05 have some spurious smaller eddies attached to the large downstream-shed eddies, and these smaller eddies are not present in the more refined (C =.025) calculation. We believe that these smaller eddies in the former are due to numerical effects, since they are made up of relatively few ($\approx$10) strong vortex elements and disappear in the more refined calculation. Finally, the shed downstream eddies in the coarser (C =.05) calculation have less well-defined eddy centers (multiple centers, etc.) than do those for the case C =.025. This is caused by using too few total vortex elements, which has the

effect of creating artificial centers. The 6 successive portraits presented here are 5% of the total number computed, and their qualitative and quantitative structure is maintained through the run of the calculations.

For C=.01, Fig. 26c, (N_{TOT}=1943), the computed picture. Although the eddy centers are well-defined, with few smaller spurious eddies, the boundaries between eddy structures blurs. We hypothesized that this was due to a problem with the time step. At high Reynolds numbers, the size of the random step taken to approximate the diffusion equation is small compared to the error in the time integration scheme used for the advection step, in contrast to the low Reynolds number situation described earlier. When a large number of vortex elements are used to resolve the boundary layer, many of them start off close together. Since the vortex method has an artificial diffusion error associated with time integration along particle trajectories (see [42]), with too large a time step the boundaries of the eddy structures diffuse and merge.

The obvious test to check this hypothesis is to reduce the time step. First, however, we change the sheet length to make sure that the discretization of the no-slip sheet at the boundary is not the reason for this smearing of vortex structures. With h reduced from .2 to .1, although the total number of sheets created is about the same, more are created along the boundary and fewer normal to the boundary. In Figure 27, we show the results for C=.05, .025, and .01, h=.1 (sheets half as long) and Δt=.05. In Fig. 27a, C=.05, (N_{TOT}=821), the spurious attached smaller eddies, multiple centers and jagged contours are all present. In Fig. 27b, C=.025, (N_{TOT}=1061), the eddy contours are smoother, with better defined centers and fewer spurious eddies. In Fig. 27c, C=.01, (N_{TOT}=1754), once again there are distinct eddy centers and smoother contours, but significant smearing between the structures.

We then decreased the time step by a factor of 2, and repeated the above calculations. In Figure 28, we show results for C=.05, .025, and .01, h=.2, and Δt=.025. In Fig. 28a, C=.05, (N_{TOT}=651), we have distinct structures, but rough contours, spurious eddies and

multiple centers. In Fig. 28b, $C=.025$, ($N_{TOT}=1096$), contours are smoother, and eddy centers and boundaries are better defined. In Fig. 28c, $C=.01$, ($N_{TOT}=2045$), contours are still smooth and centers and boundaries are well-defined. Thus, with a smaller time step, boundary merging did not occur and vortex structures remain distinct.

To check this result, we halved the sheet length and repeated the above calculation. In Figure 29, we show results for $C=.05$, .025 and .01, $h=.1$ and $\Delta t=.025$. For all three cases, $C=.05$ ($N_{TOT}=1069$), $C=.025$ ($N_{TOT}=1226$) and $C=.01$ ($N_{TOT}=2146$), the same progression is present, with no boundary smearing for the $C=.01$ case. To summarize, in this unsteady regime, more vortices provide better resolution of the large vortex structures, however there is an accompanying requirement that the time step be suitably decreased so that the advection error remains small in comparison with the physical diffusion scale.

Given this analysis of the effect of changing numerical parameters on large-scale eddy structures, we now consider the velocity field itself. Here, we want to study the convergence of the time-averaged velocity profile to see if the same conclusions hold about the effects of the choice of numerical parameters. In an unsteady flow, particular care must be taken to determine the length of the averaging window. For example, in the case $C=.05$, $h=.2$, $\Delta t=.05$, approximately three complete eddy shedding cycles occurred during the 500 time step fully developed flow period. If one attempts to compute an average velocity profile over the full 500 time steps, the profile obtained greatly depends on whether one is "in phase" with the cycling frequency. As an illustration, consider a function $f(i)$ defined on the positive integers i, where i is time in integer units, and suppose $f(i)=0$ if i is odd and $f(i)=1$ if i is even. If one attempts to compute an average value of f over an averaging window of 3 units, the answer depends on whether one starts at an odd or an even integer.

Since we could not afford to perform a calculation for each of the 12 parameter combinations over 20 – 30 shedding cycles, after much experimentation we chose the following approach. For each data set, start the time window when the center of the first eddy passes

W_{END} and stop the averaging window when the next shed eddy reaches W_{END}. Calling this one cycle, compute the average velocity profile over this cycle and store it. Starting with the second eddy, begin another averaging window which ends when the center of the third eddy reaches W_{END} and compute the average velocity profile over this second cycle. Do this until all the eddies have been shed in the data set under study, and compute a velocity profile by averaging over all the individual one cycle averages. There were typically $3-4$ one cycle averages in each grand average portrait.

In Figure 30, we show the streamline plots of these average velocity fields for all combinations of $C=.05,\ .025,\ .01,\ h=.2,\ .1$, and $\Delta t=.05,\ .025$. The previous conclusions about the choice of numerical parameters are reinforced. For the crudest calculations, a jagged, multiple center, single recirculation zone is seen with reattachment length of about 8 step heights. As the number of vortices is increased (C decreased), the average profile becomes a single, smoother, large recirculation zone with a well-defined single center and similar reattachment length. For $C=.01$ with $\Delta t=.05$ and both $h=.2$ and $h=.1$, this portrait is lost and the results are ambiguous; but halving the time step ($C=.01$, $\Delta t=.025$, $h=.2$ and $h=.1$) brings back the single eddy, single center, smooth recirculation zone with a reattachment length of about 8.5 step heights.

VII. SUMMARY

We have studied the convergence of the vortex method applied to two-dimensional, viscous, incompressible flow over a backwards-facing step. Calculations were performed over a wide range of Reynolds numbers. At low Reynolds number, where the real solution is steady, we showed that the most important parameter is the circulation of an individual vortex element, which controls the total number N of vortex elements. Within the laminar regime, reductions in the time step and sheet length are of secondary importance. Convergence was

demonstrated using a variety of measurements, from integrated quantities such as total circulation to pointwise measurements such as eddy centers and reattachment points. We showed that the variance from the mean decays as $1/N$ for both the velocity field and the total circulation. Our predictions of recirculation zone size and length were in excellent agreement with experiment.

For higher Reynolds number calculations, we demonstrated convergence for averaged quantities such as average velocity profiles and eddy boundaries. Here, while the total number of vortex elements controlled the accuracy, the time step also must be decreased. With suitable refinement of the relevant numerical parameters, we showed that the dynamics of large fluid structures may be accurately computed. We did not try to analyze our data at high Reynolds number with pointwise instantaneous measurements, since the underlying equations are unstable to small perturbations. The calculations in this paper demonstrate that these perturbations organize themselves into coherent structures whose size and dynamics remain unchanged as the numerical parameters are refined. The problems of identifying, classifying and tracking these coherent structures will be discussed in a later paper [40].

Acknowledgements: The comments and suggestions of Alexandre Chorin and Ole Hald are gratefully acknowledged. All calculations were performed at the Lawrence Berkeley Laboratory, University of California, Berkeley.

REFERENCES

1) D.E. Abbot and S.J. Kline, *Experimental investigation of subsonic turbulent flow over single and double backward facing steps,* Journal of Basic Engineering, (1962), 317-325.

2) C. Anderson and C. Greengard, *On vortex methods,* SIAM J. Numer. Anal., **22** (1985), pp. 413 - 440.

3) B.F. Armaly, F. Durst, J.C.F. Pereira and B. Schonung, *Experimental and theoretical investigation of backward-facing step flow,* J. Fluid Mech., **127,** (1983), pp.473-496.

4) W.T. Ashurst, *Calculation of plane sudden expansion flow via vortex dynamics,* 2nd Sympoisum on Turbulent Shear Flows, London, July 1979.

5) J.T. Beale and A. Majda, *Vortex methods. I: Convergence in three dimensions,* Math. Comp. **39** (1982), pp. 1 - 27.

6) J.T. Beale and A. Majda, *Vortex methods. II: Higher order accuracy in two and three dimensions,* Math. Comp. **39** (1982), pp. 29 - 52.

7) P. Bradshaw and F.Y.F. Wong, *The reattachment and relaxation of a turbulent shear layer,* J. Fluid. Mech., **52,** (1972), pp.113-135.

8) I.P. Castro, *The numerical prediction of recirculating flows,* Proc. Int. Conf. Num. Meth. in Laminar and Turbulent Flow, (Eds. C. Taylor and K. Morgan), Pentech Press, London, (1978), pp. 329-339.

9) A.Y. Cheer, *A study of incompressible 2-D vortex flow past a circular cylinder,* SIAM J. Sci. Statist. Comput., **4** (1983), pp.685-705.

10) A.J. Chorin, *Numerical study of slightly viscous flow,* J. Fluid Mech., **57** (1973), pp. 785 - 796.

11) A.J. Chorin, *Vortex sheet approximation of boundary layers* J. Comp. Phys., **27** (1978), 428-442.

12) V.M. Del Prete and O.H. Hald, *Convergence of vortex methods for Euler's equations,* Math. Comp., **32** (1978), pp 791 - 809.

13) M.K. Denham and M.A. Patrick, *Laminar flow over a downstream-facing step in a two-dimensional flow channel,* Trans. Instn. Chem. Engrs., **52,** (1974), pp.361-367.

14) F. Durst and C. Tropea, *Flows over two-dimensional backward-facing steps,* Structure of Complex Turbulent Shear Flows (R. Dumas and L. Fulachier, Eds.), IUTAM Symposium, Springer-Verlag, Berlin, (1982).

15) J.K. Eaton and J.P Johnston, *Low frequency unsteadyness of a reattaching turbulent shear layer* in "Turbulent Shear Flows 3" (Editors, L.J.S. Bradbury et. al.), Springer-Verlag, New York (1982).

16) D.W. Etheridge and P.H. Kemp, *Measurements of turbulent flow downstream of a rearward-facing step,* Journal of Fluid Mechanics, **86, part 3,** (1978), pp. 545-566.

17) A.F. Ghoniem, A.J. Chorin and A.K. Oppenheim, *Numerical modeling of turbulent flow in a combustion tunnel,* Philos. Trans. Roy. Soc. London, **A304,** (1982), pp. 303-325.

18) A.F. Ghoniem and J.A. Sethian, *Dynamics of turbulent structure in a recirculating flow: a computational study,* AIAA 23rd Aerospace Sciences Meeting, (1985), AIAA-85-0146, to appear in AIAA Journal.

19) R.J. Goldstein, V.L. Eriksen, R.M. Olson, E.R.G. Eckert, *Laminar separation, reattachment and transition of the flow over a downstream-facing step* Transactions of the ASME, (1970), pp.732-741.

20) J. Goodman, *Convergence of the random vortex method,* preprint.

21) L.P. Hackman, G.D. Raithby, and A.B. Strong, *Numerical prediction of flow over a backwards-facing step,* Int. Jour. Num. Meth. Fluids, **4** (1984), pp. 711-724.

22) O.H. Hald, *Convergence of vortex methods for Euler's equations, II,* SIAM J. Numer. Anal., **16** (1979), pp. 726 - 755.

23) O.H. Hald, *Convergence of Fourier methods for Navier-Stokes* equations, J. Comp. Phys., **40** (1981), pp. 305 - 317.

24) O.H. Hald, *The flowmap for Euler's equations,* to be published.

25) H. Honji, *The starting flow down a step,* J. Fluid Mech., **69,** (1975), pp.229-240.

26) J.P. Johnston, *Internal flows,* in "Turbulence", (Editors P. Bradshaw), Springer-Verlag, 1978.

27) R. Krasny, *Desingularization of periodic vortex sheet roll-up* J. Comp. Phys., in press.

28) J.L. Kueny and G. Binder, *Viscous flow over backward facing steps; an experimental investigation,* preprint.

29) L.D. Landau and E.M. Lifshitz, *Fluid Mechanics,* Pergammon, New York, 1975.

30) A. Leonard, *Vortex methods for flow simulation,* J. Comp. Phys., **37** (1980), pp. 289 - 335.

31) A. Leonard, *Review of Vortex Methods,* in "Annual Review of Fluid Mechanics", (Eds. Van Dyke, Wehausen, Lumley), Annual Reviews, Palo Alto, CA., 1985.

32) M.A. Leschziner, *Practical evaluation of three finite difference schemes for the computation of steady-state recirculating flows,* Computer Methods in Applied Mechanics and Engineering, **23,** (1980), pp.293-312.

33) A. Majda and J.A. Sethian, *The derivation and numerical solution of the equations for zero mach number* combustion, Combust. Sci. Tech., **42,** (1985), pp. 185-205.

34) C. Marchioro and M. Pulvirenti, *Hydrodynamics in two dimensions and vortex theory,* Comm. Math. Phys., **84,** (1982), pp.483-503.

35) M.F. McCracken and C.S. Peskin, *A vortex method for blood flow through heart valves,* J. Comp. Phys., **35** (1980), pp. 183-205.

36) W.D. Moss, S. Baker, L.J.S. Bradbury, *Measurements of mean velocity and Reynolds stresses in some regions of recirculating flow,* in "Turbulent Shear Flows I", (Editors, F.Durst et. al.), Springer-Verlag, 1979.

37) J. Periaux, O. Pironneau, F. Thomasset, *Computational results of the back step flow workshop,* Fifth International GAMM Conference on Numerical Methods in Fluid Mechanics, Springer-Verlag, 1983. **9,** (1976), pp.75-103.

38) M. Perlman, *On the accuracy of vortex methods,* J. Comp. Phys., **59** (1985),pp. 200-223.

39) S. Roberts, *Accuracy of the random vortex method for a problem with non-smooth initial conditions,* J. Comp. Phys., **58** (1985), pp.29-43.

40) J.A. Sethian, *Identifying and tracking coherent structures in turbulent flow,* in progress.

41) J.A. Sethian, *Numerical simulation of flame propagation in a closed vessel,* Proc. Fifth Int. GAMM Conf. Numer. Meth. Fluid Mech., Rome, Italy, (1983)

42) J.A. Sethian, *Turbulent combustion in open and closed vessels,* J. Comp. Phys., **55,** (1984), pp.425-456.

43) J.A. Sethian, *Vortex methods and turbulent combustion,* Lectures in Applied Mathematics, **22,** (1985).

44) J.A. Sethian, *The wrinkling of a flame due to viscosity,* Fire Dynamics and Heat Transfer, (J. Quintiere, Ed.), Proc. 21st Nat. Heat. Transfer Conf., (1983), pp. 29.

EQUATIONS OF MOTION

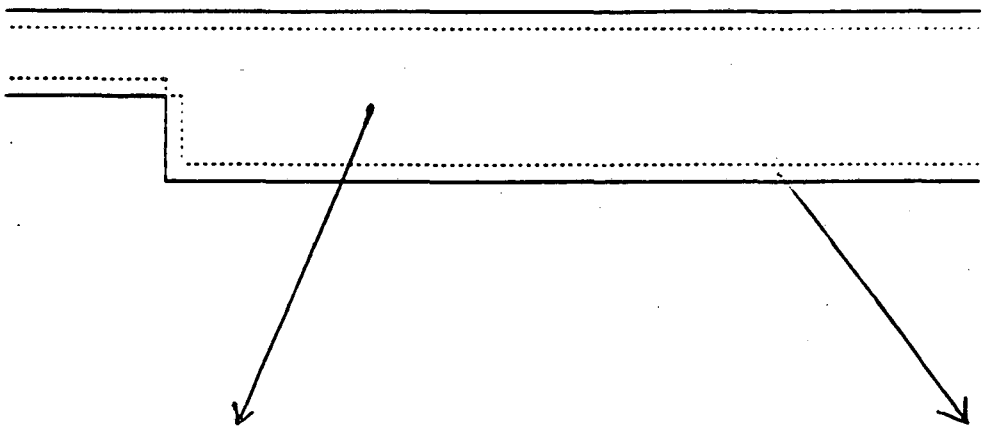

INTERIOR

BOUNDARY LAYER

Advection: $\partial_t \xi = -(\vec{u} \cdot \nabla)\xi$

$\nabla \cdot \vec{u} = 0$

$\xi = \nabla \times \vec{u}$

Diffusion: $\partial_t \xi = (1/R)\nabla^2 \xi$

Advection: $\partial_t \xi = -(u \cdot \nabla)\xi$

$\nabla \cdot \vec{u} = 0$

$\xi = -\partial u / \partial y$

Diffusion: $\partial_t = (1/R)\partial_\xi^2 / \partial_y^2$

FIGURE 1

NUMERICAL PARAMETERS

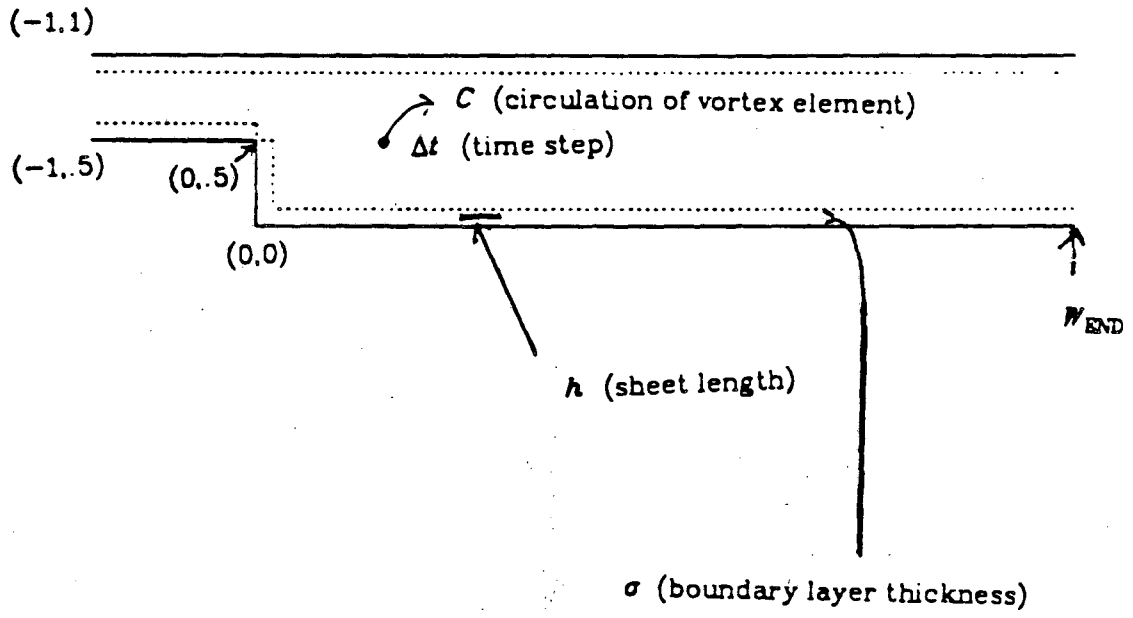

FIGURE 2

STARTUP OF FLOW $R = 50$

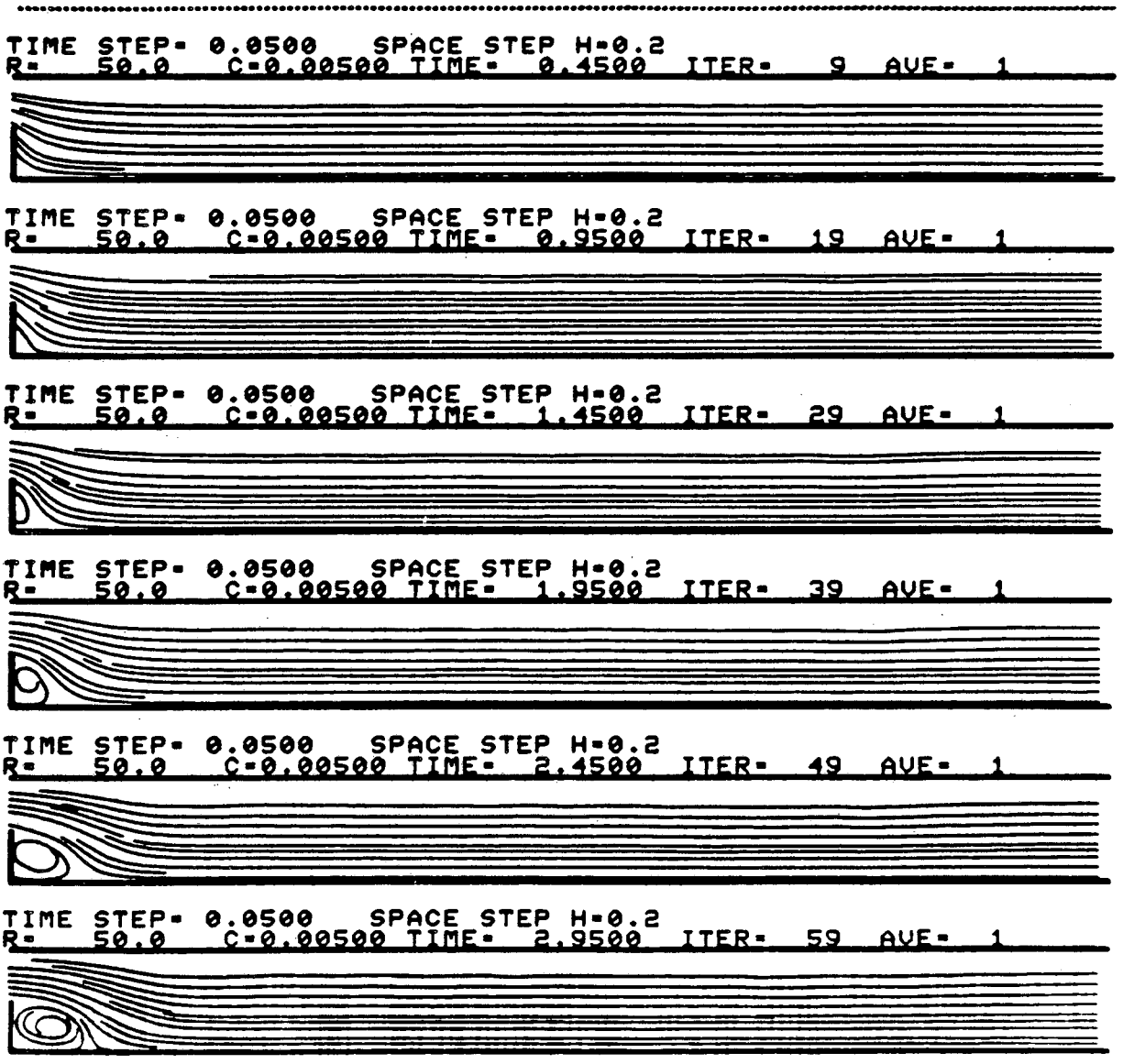

FIGURE 3

SUCCESSIVE TIME PORTRAITS OF FULLY DEVELOPED FLOW $R = 50$

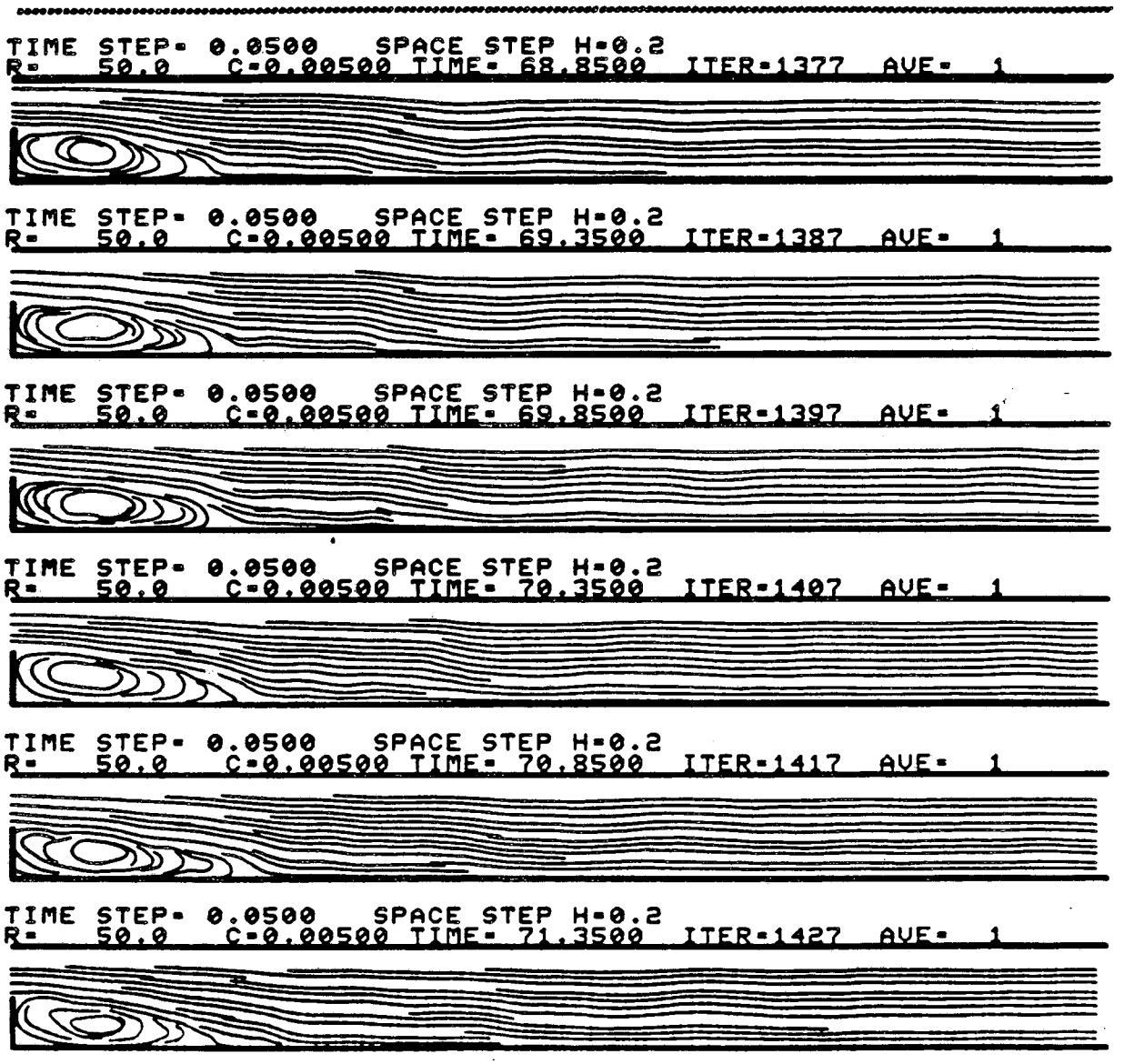

FIGURE 4

AVERAGED STREAMLINES OVER 2000 TIME STEPS $R = 50$

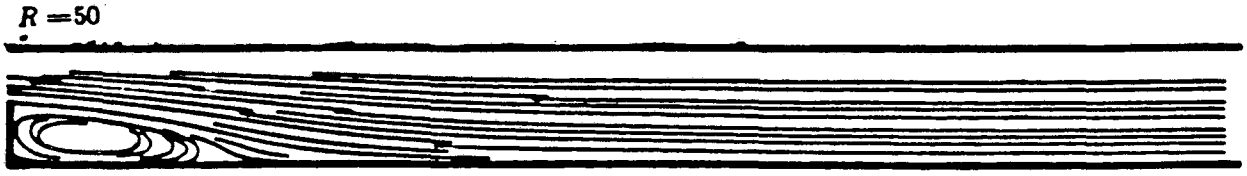

FIGURE 5

SUCCESSIVE TIME PORTRAITS OF FULLY DEVELOPED FLOW $R = 125$

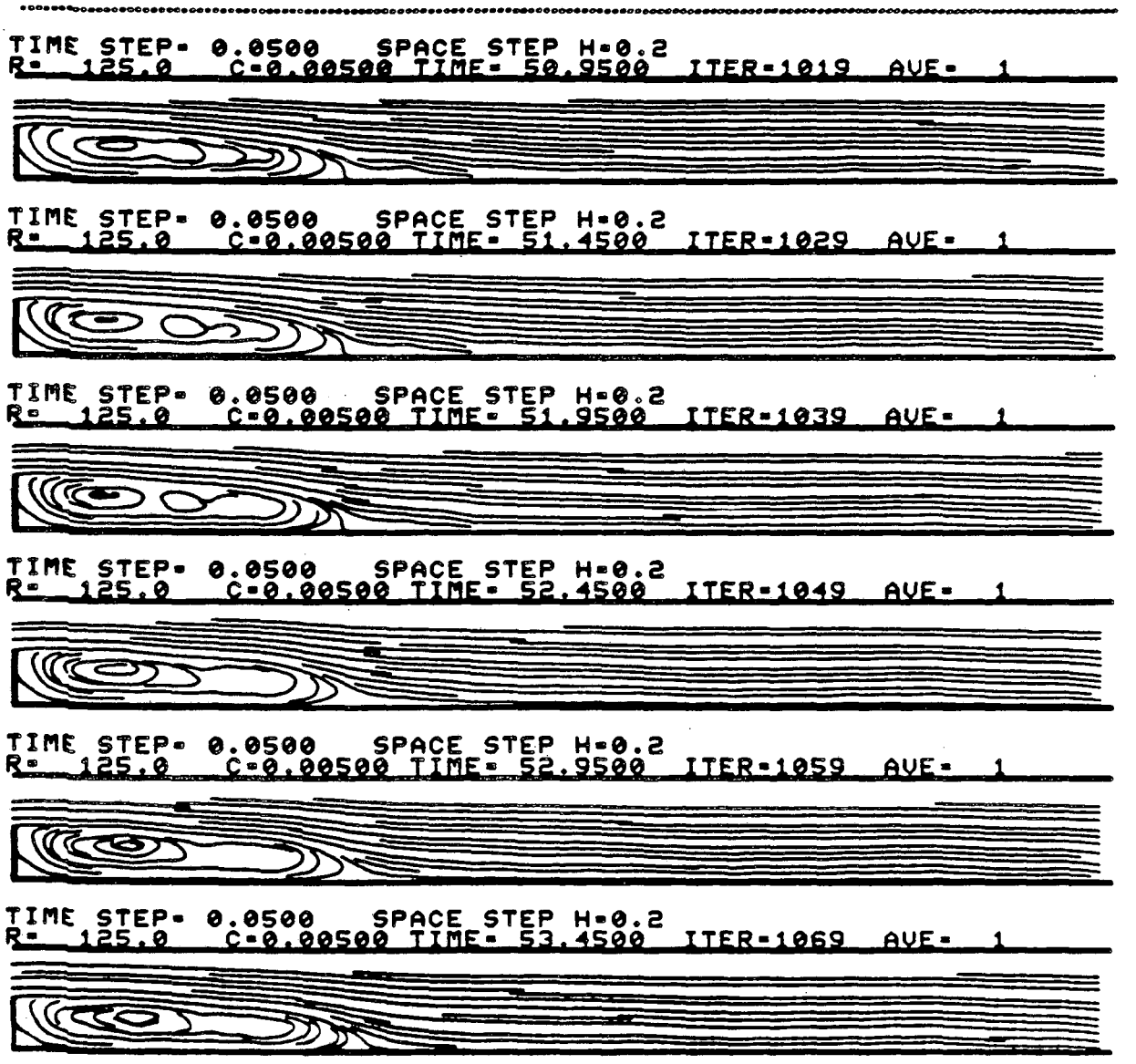

FIGURE 6

SUCCESSIVE TIME PORTRAITS OF FULLY DEVELOPED FLOW $R = 500$

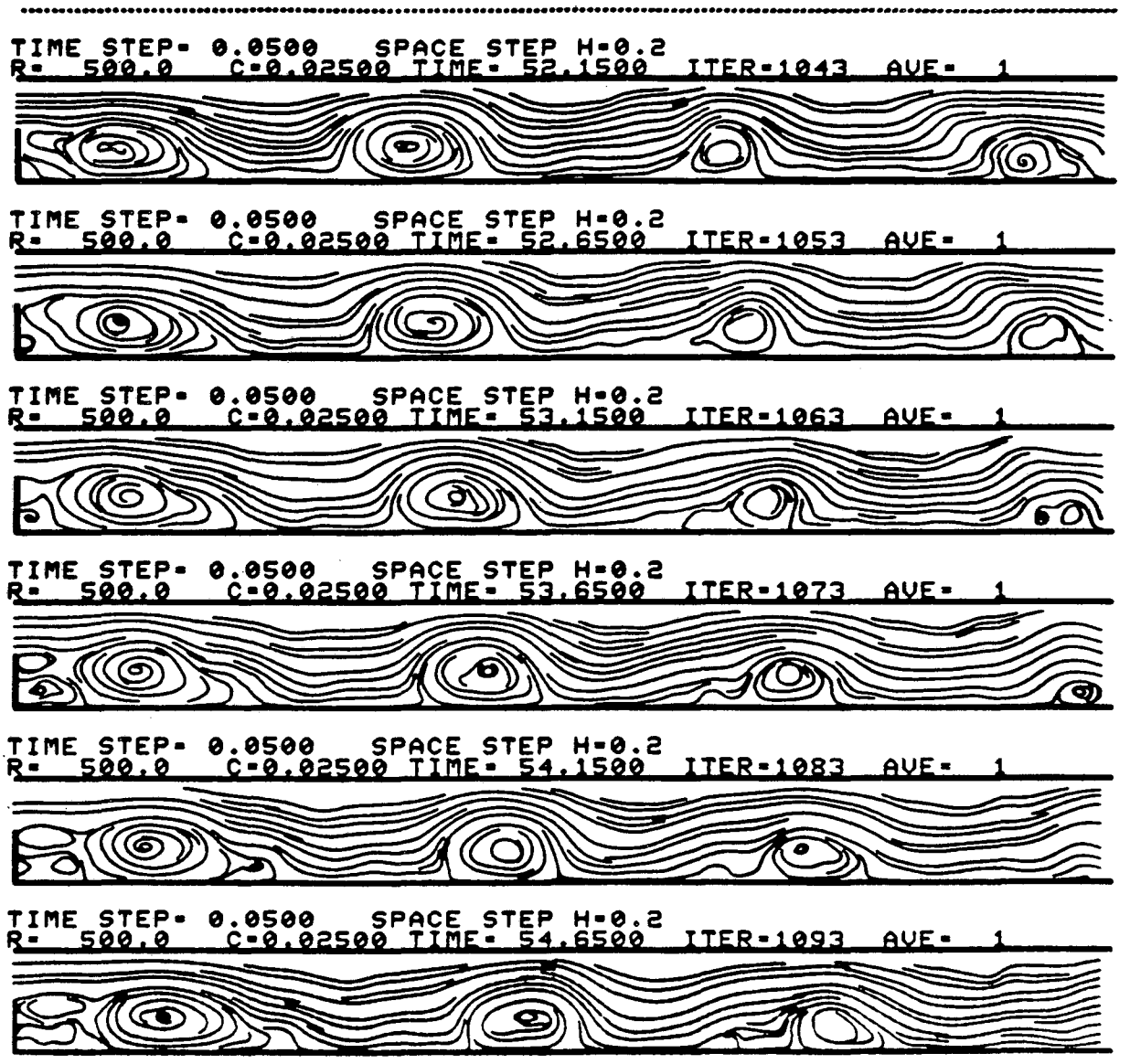

FIGURE 7

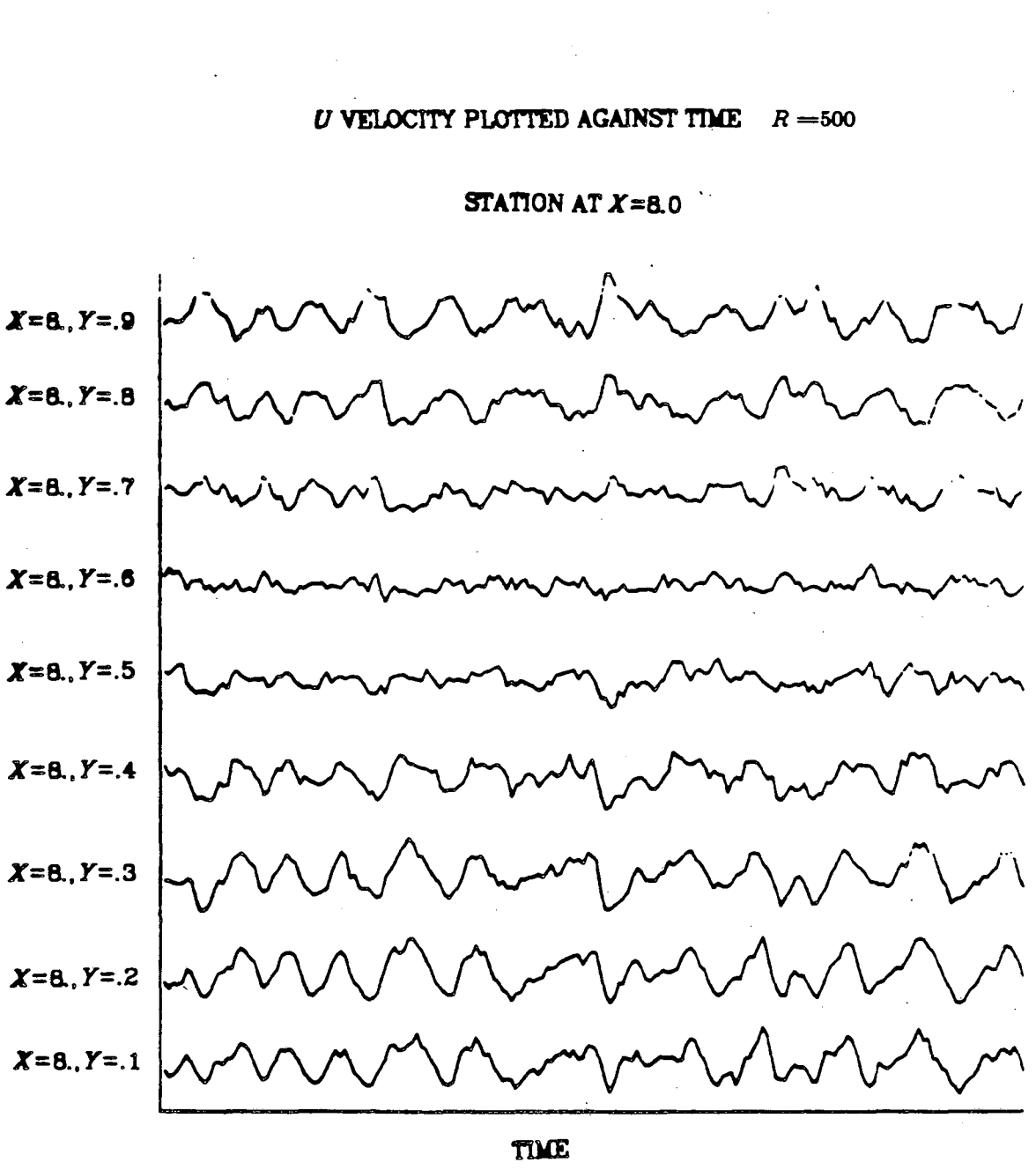
U VELOCITY PLOTTED AGAINST TIME R =500
STATION AT X=8.0
X=8., Y=.9
X=8., Y=.8
X=8., Y=.7
X=8., Y=.6
X=8., Y=.5
X=8., Y=.4
X=8., Y=.3
X=8., Y=.2
X=8., Y=.1
TIME

FIGURE 8

SUCCESSIVE TIME PORTRAITS OF FULLY DEVELOPED FLOW $R = 375$

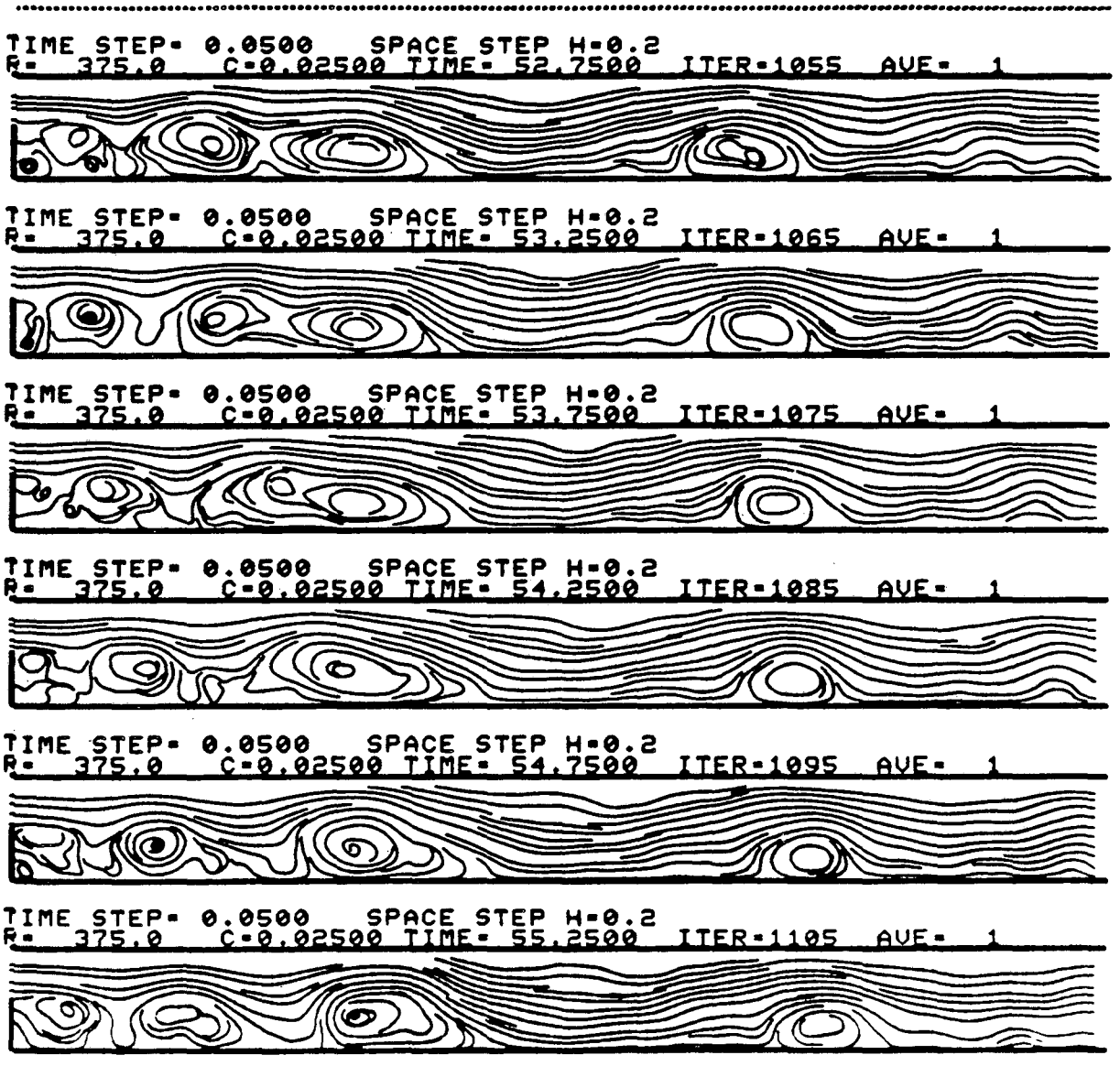

FIGURE 9

SUCCESSIVE TIME PORTRAITS OF FULLY DEVELOPED FLOW $R = 250$

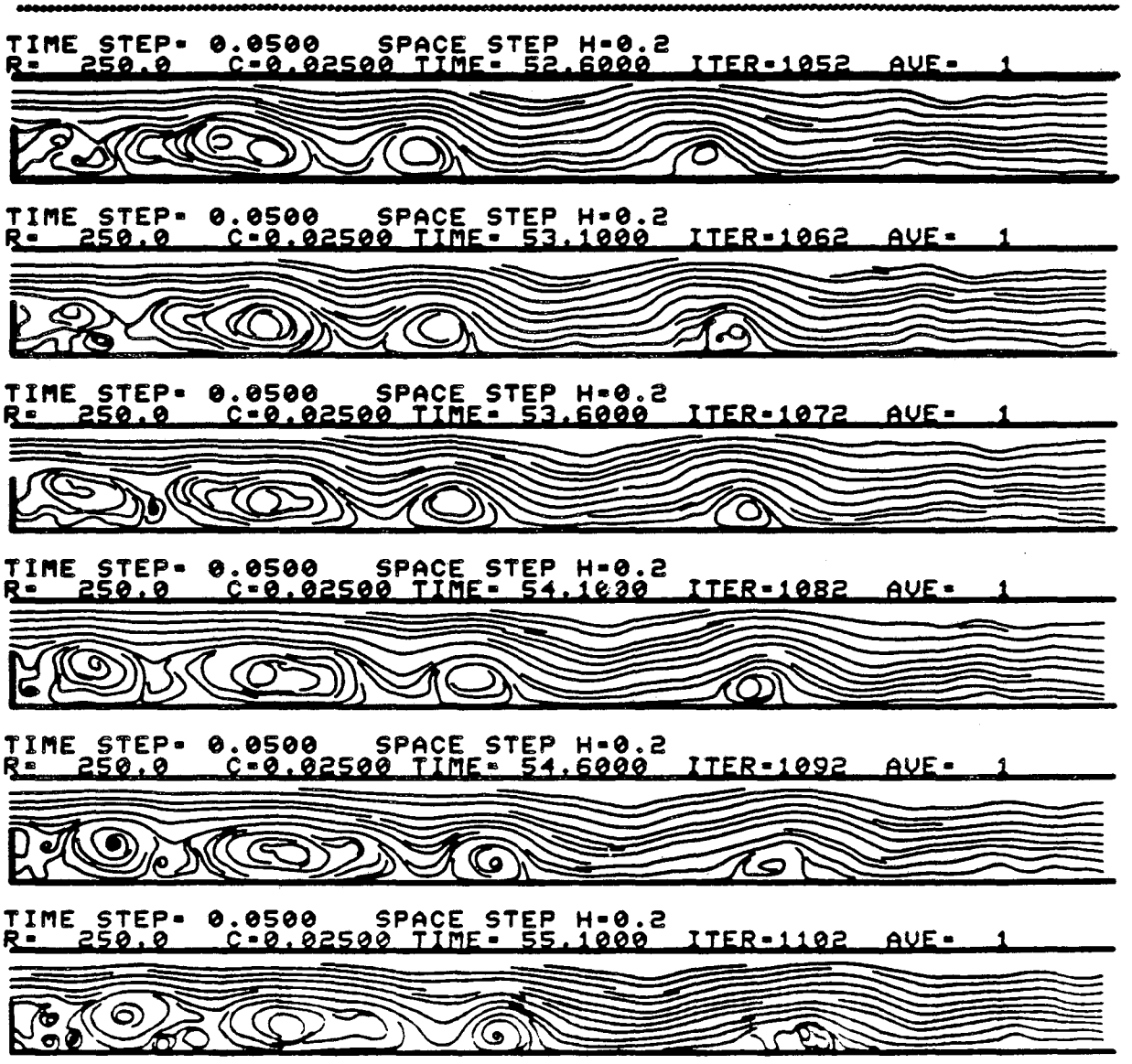

FIGURE 10

BLOW-UP OF CORNER FOR $R = 500$

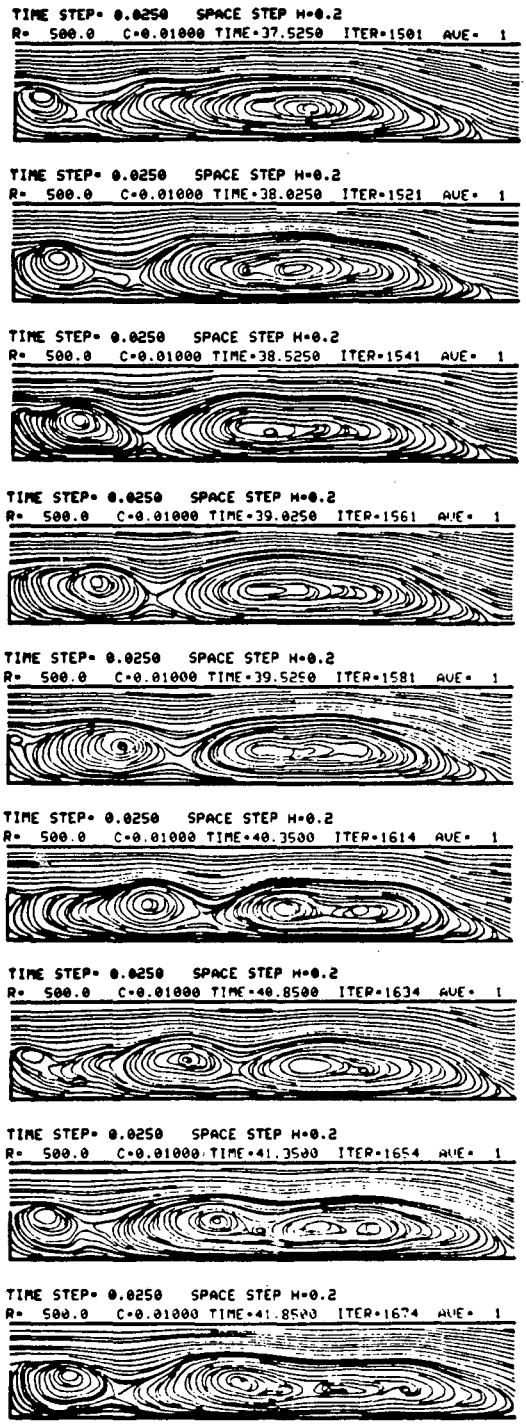

FIGURE 11

SUCCESSIVE TIME PORTRAITS OF FULLY DEVELOPED FLOW $R = 5000$

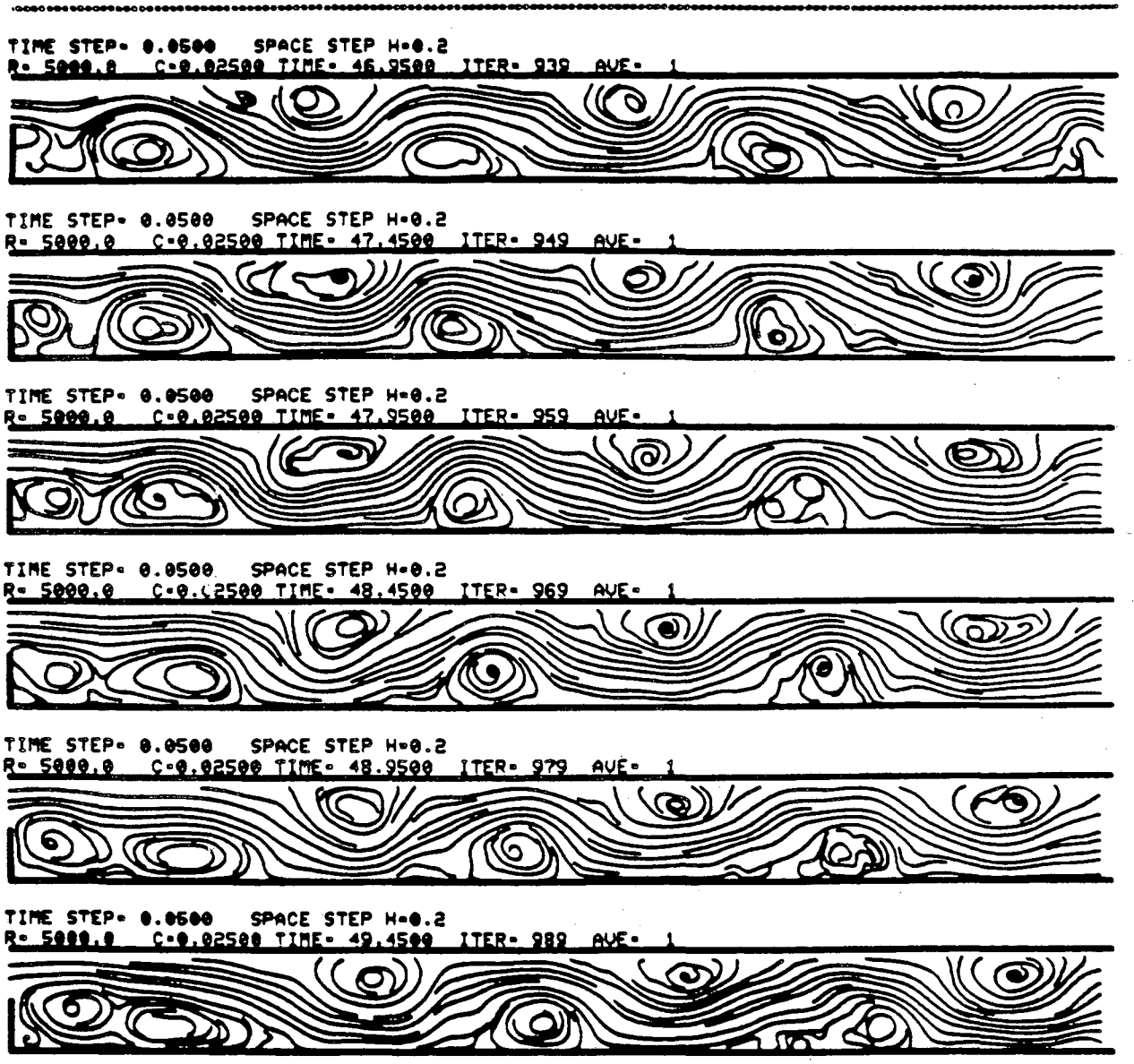

FIGURE 12

AVERAGED STREAMLINES OVER 2000 TIME STEPS

R =50, 125, 250, 375, 500, 5000

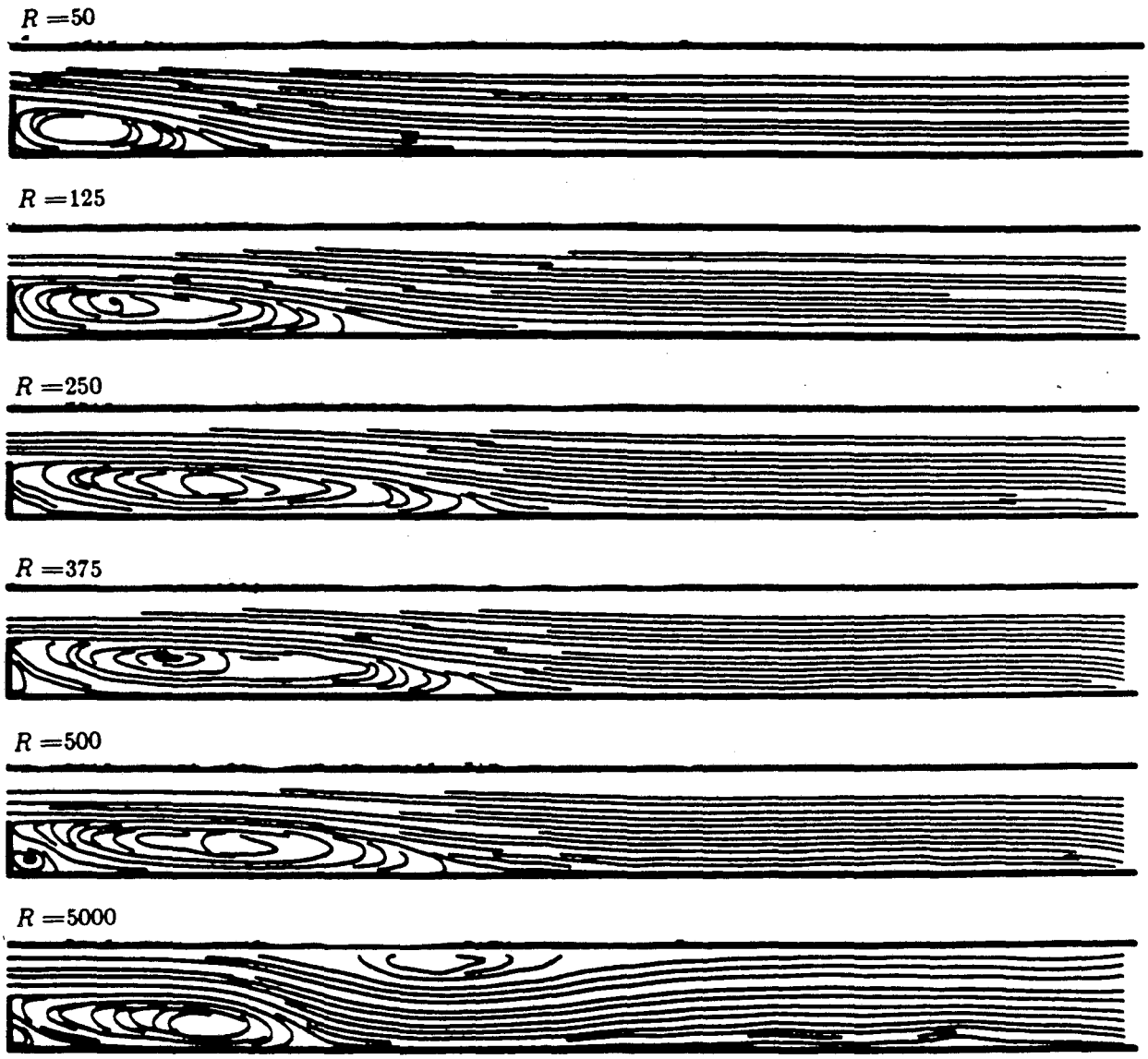

FIGURE 13

REATTACHMENT LENGTH AS A FUNCTION OF REYNOLDS NUMBER

R =50, 125, 250, 375, 500, 5000

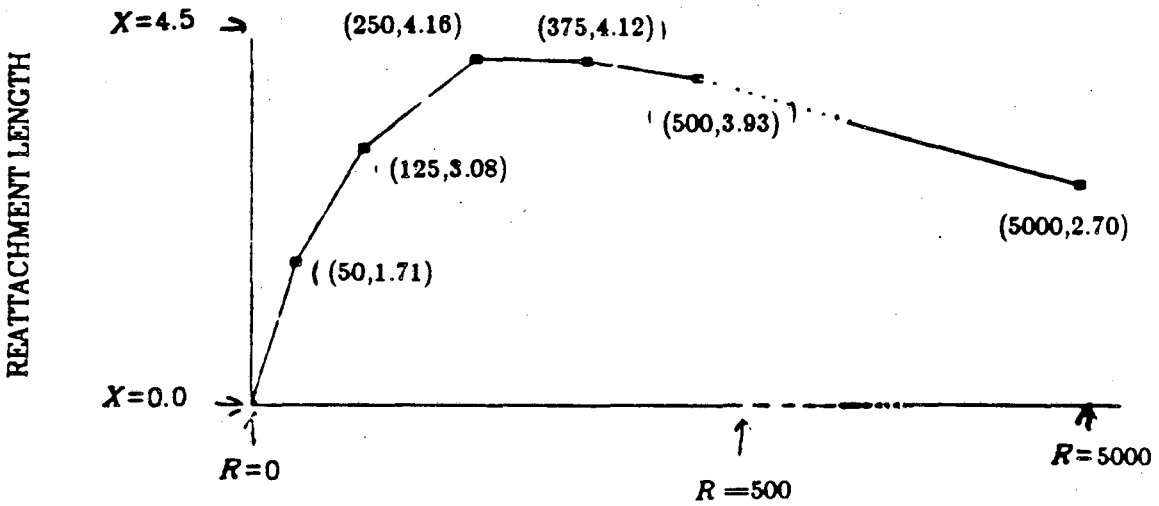

REYNOLDS NUMBER

FIGURE 14

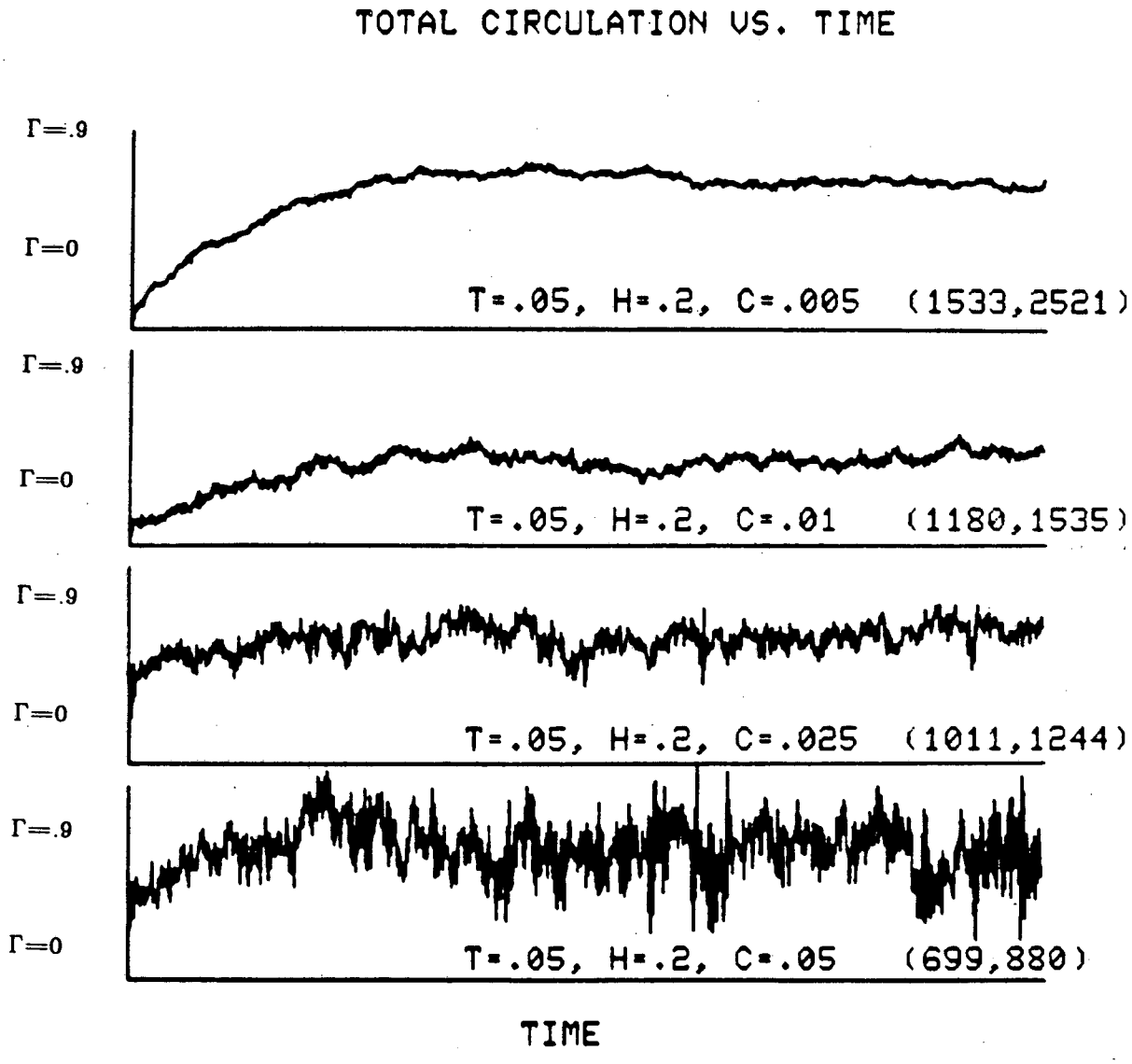
TOTAL CIRCULATION VS. TIME
Γ=.9
Γ=0
T=.05, H=.2, C=.005 (1533,2521)
Γ=.9
Γ=0
T=.05, H=.2, C=.01 (1180,1535)
Γ=.9
Γ=0
T=.05, H=.2, C=.025 (1011,1244)
Γ=.9
Γ=0
T=.05, H=.2, C=.05 (699,880)
TIME

FIGURE 15

DECAY OF CIRCULATION VARIANCE AS A FUNCTION OF NUMBER OF VORTICES

$$\text{Circulation Variance} = \frac{1}{500} \sum_{n=500}^{1000} |\Gamma(n\,\Delta t) - \bar{\Gamma}|^2$$

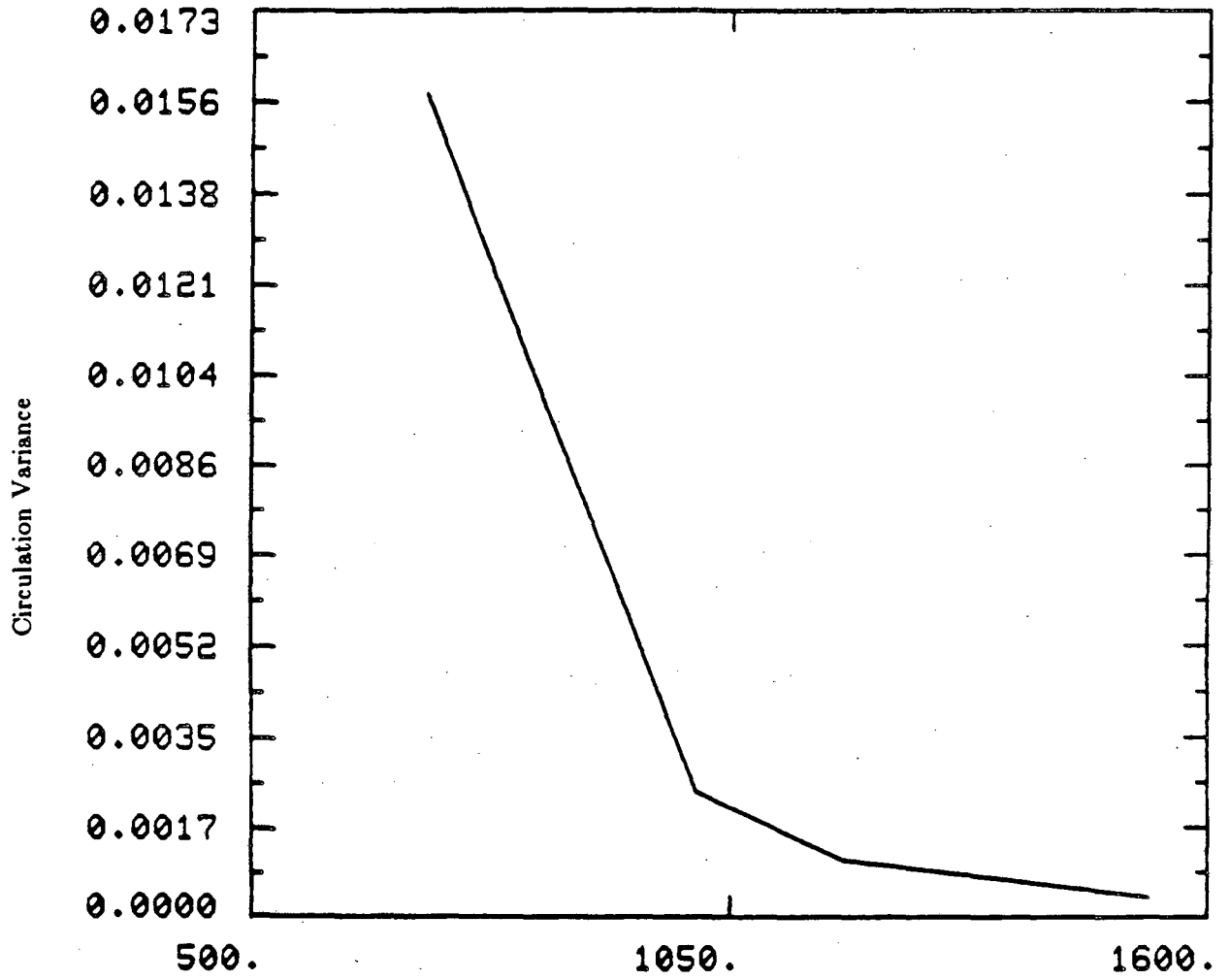

FIGURE 16

TOTAL CIRCULATION VS. TIME

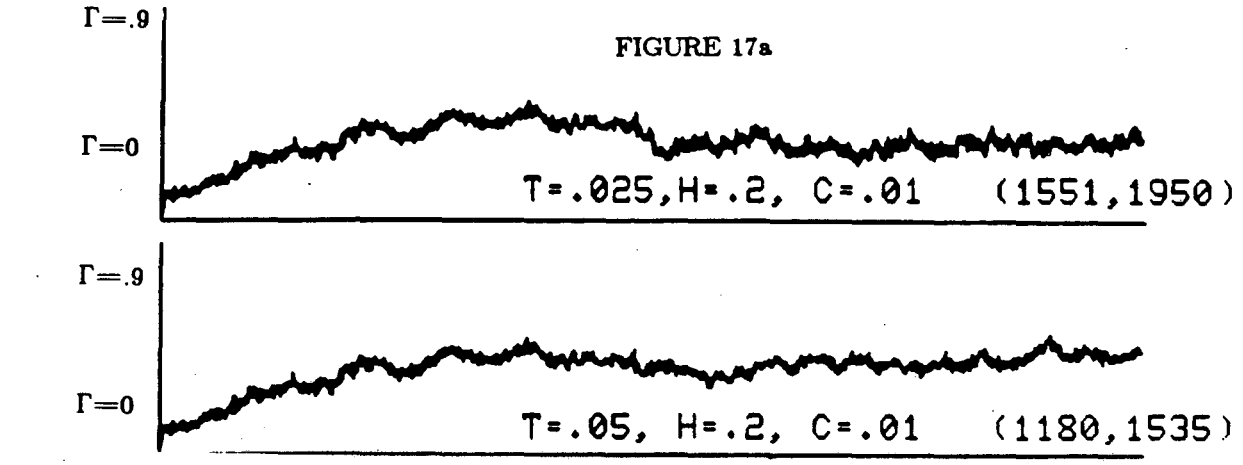

FIGURE 17a

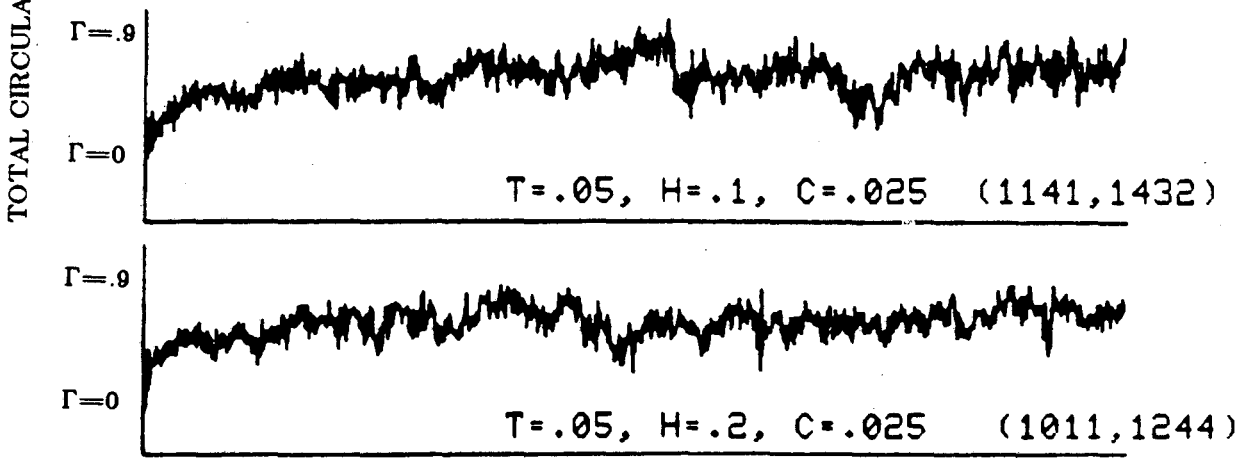

FIGURE 17b

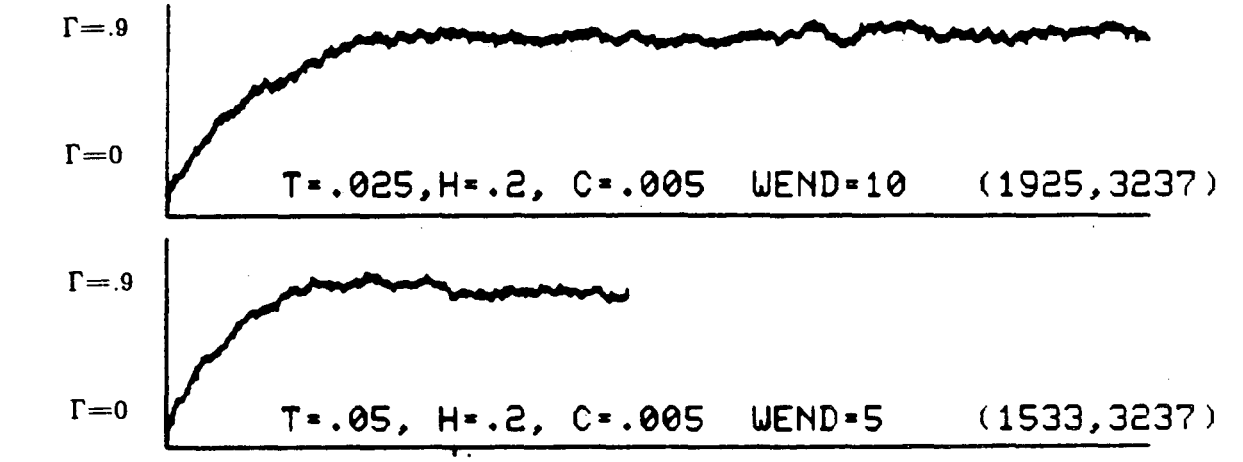

FIGURE 17c

TOTAL CIRCULATION

TIME

ERROR $Err\,(M)$ IN VELOCITY BETWEEN AVERAGING WINDOW OF SIZE M vs. FULL AVERAGE

$$Err\,(M) = \frac{1}{(\mathrm{M})(\mathrm{W}(\mathrm{M}))} \sum_{\text{windows of length M}} \left(\frac{1}{I \cdot J} \sum_{i,j} \mid \vec{u}^{\,n}_{i,j}(M) - \vec{u}^{\,n}_{i,j}(500) \mid^2\right) / \left(\mid \vec{u}^{\,n}_{i,j}(500) \mid^2\right)$$

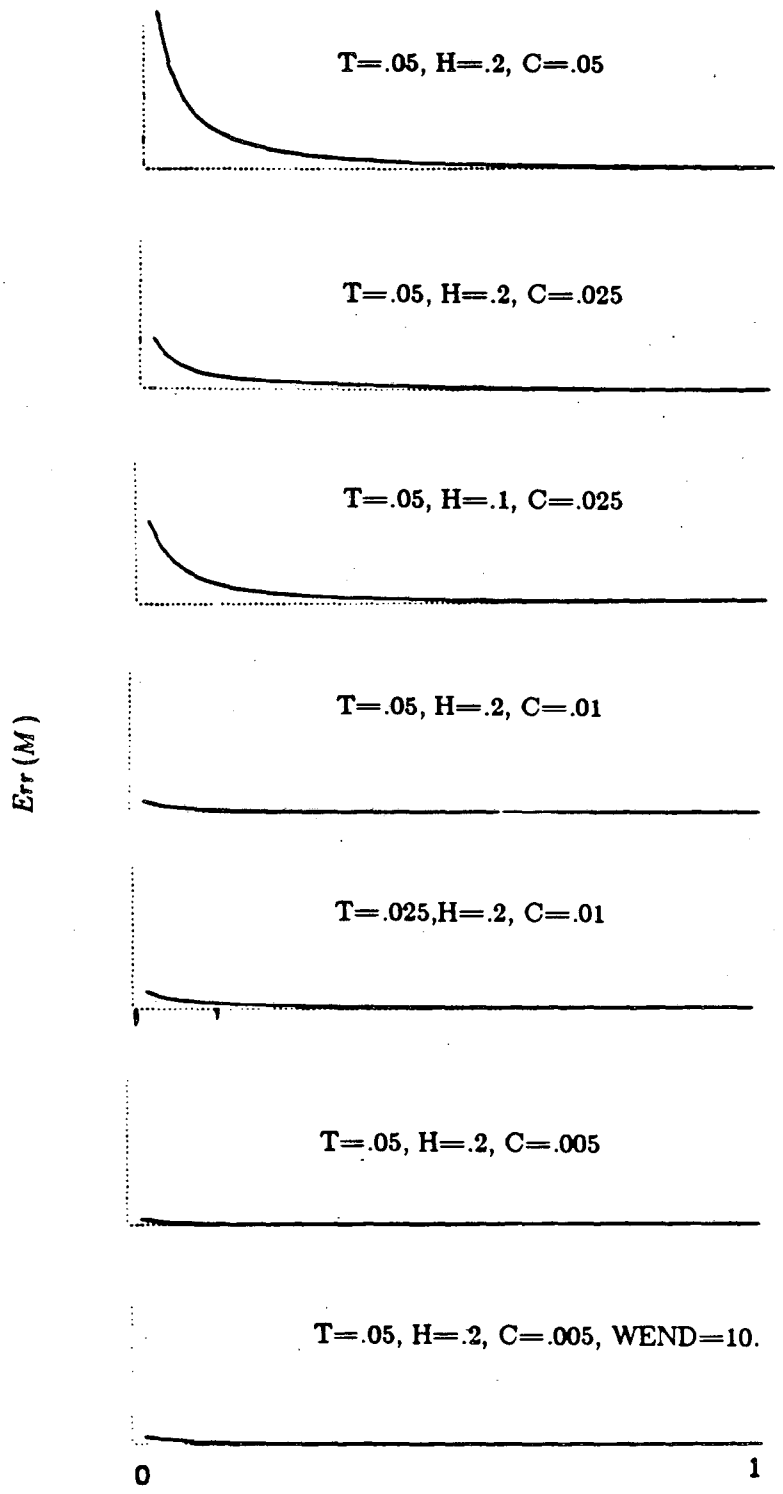

(Sample Window Size)/(Maximum Window Size) = M / 500

FIGURE 18

SPATIAL VARIANCE Var^n FROM MEAN VELOCITY AS A FUNCTION OF TIME

$$Var^n = \frac{1}{I \cdot J} \sum_{i,j} | \vec{u}^n_{i,j} - \overline{u}_{i,j} |^2$$

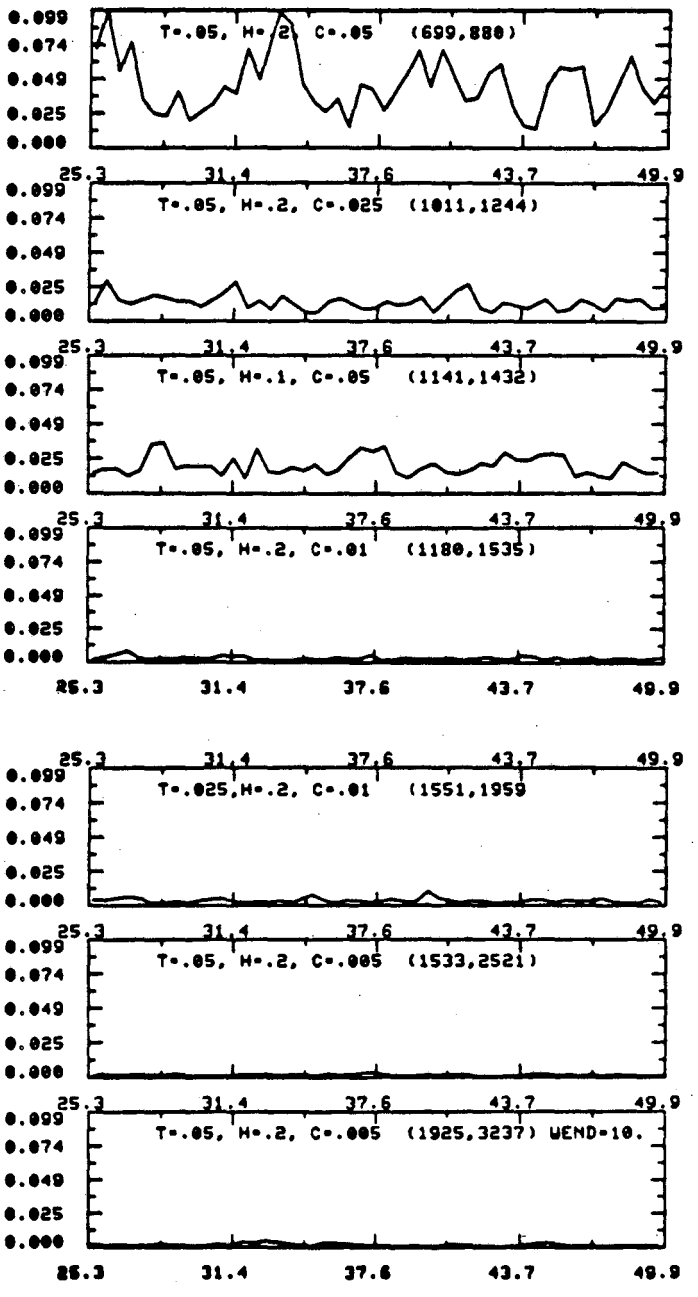

Var^n

TIME

FIGURE 19

DECAY OF TIME AVERAGED SPATIAL VARIANCE $\overline{Var}^n$ AS A FUNCTION OF NUMBER OF VORTICES

$$\overline{Var}^n = \frac{1}{500} \sum_{n=500}^{1000} \frac{1}{I \cdot J} \sum_{i,j} | \vec{u}^n_{i,j} - \overline{u}_{i,j} |^2$$

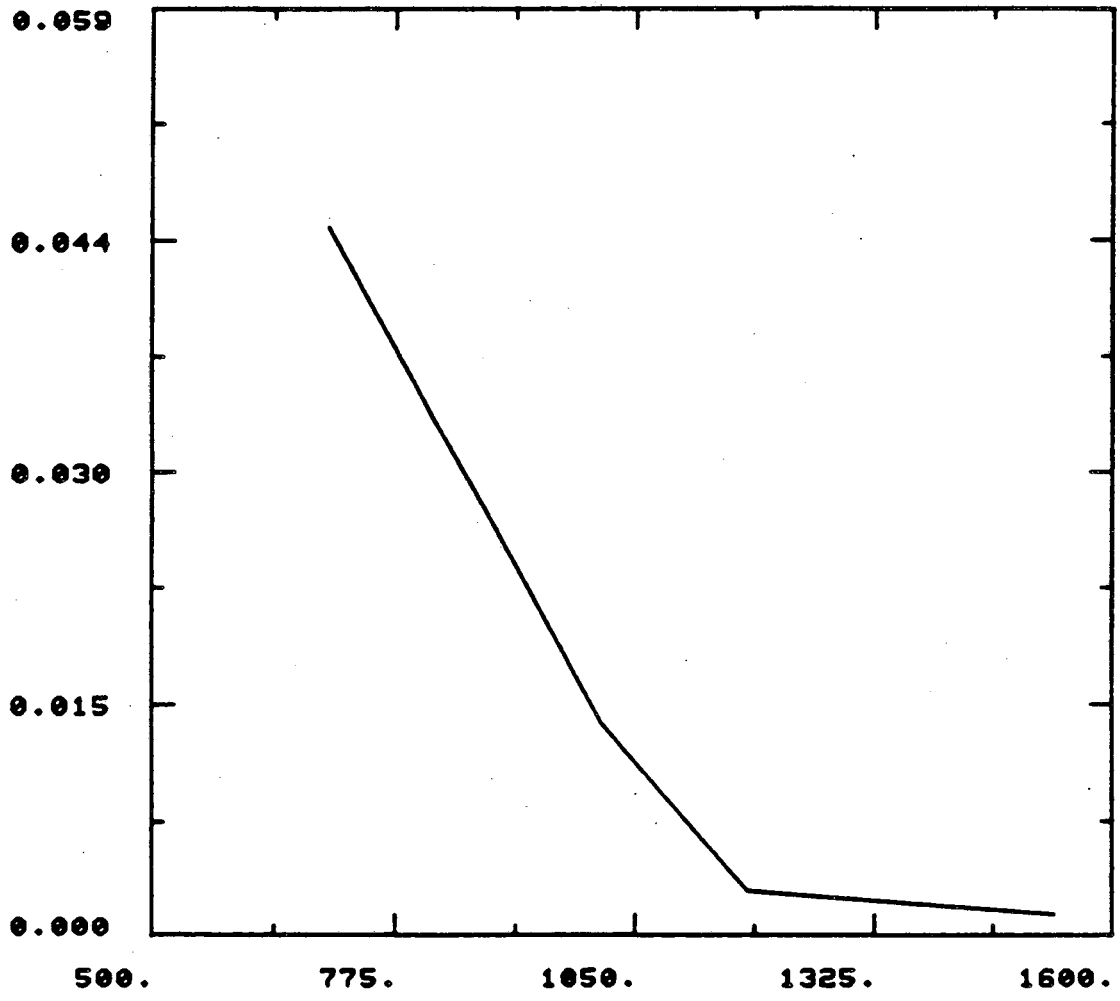

FIGURE 20

TEMPORAL VARIANCE $Var_{i,j}$ FROM MEAN AS A FUNCTION OF SPACE

$$Var_{i,j} = \frac{1}{500} \sum_{n=500}^{1000} | \vec{u}^{n}_{i,j} - \bar{\vec{u}}_{i,j} |^2$$

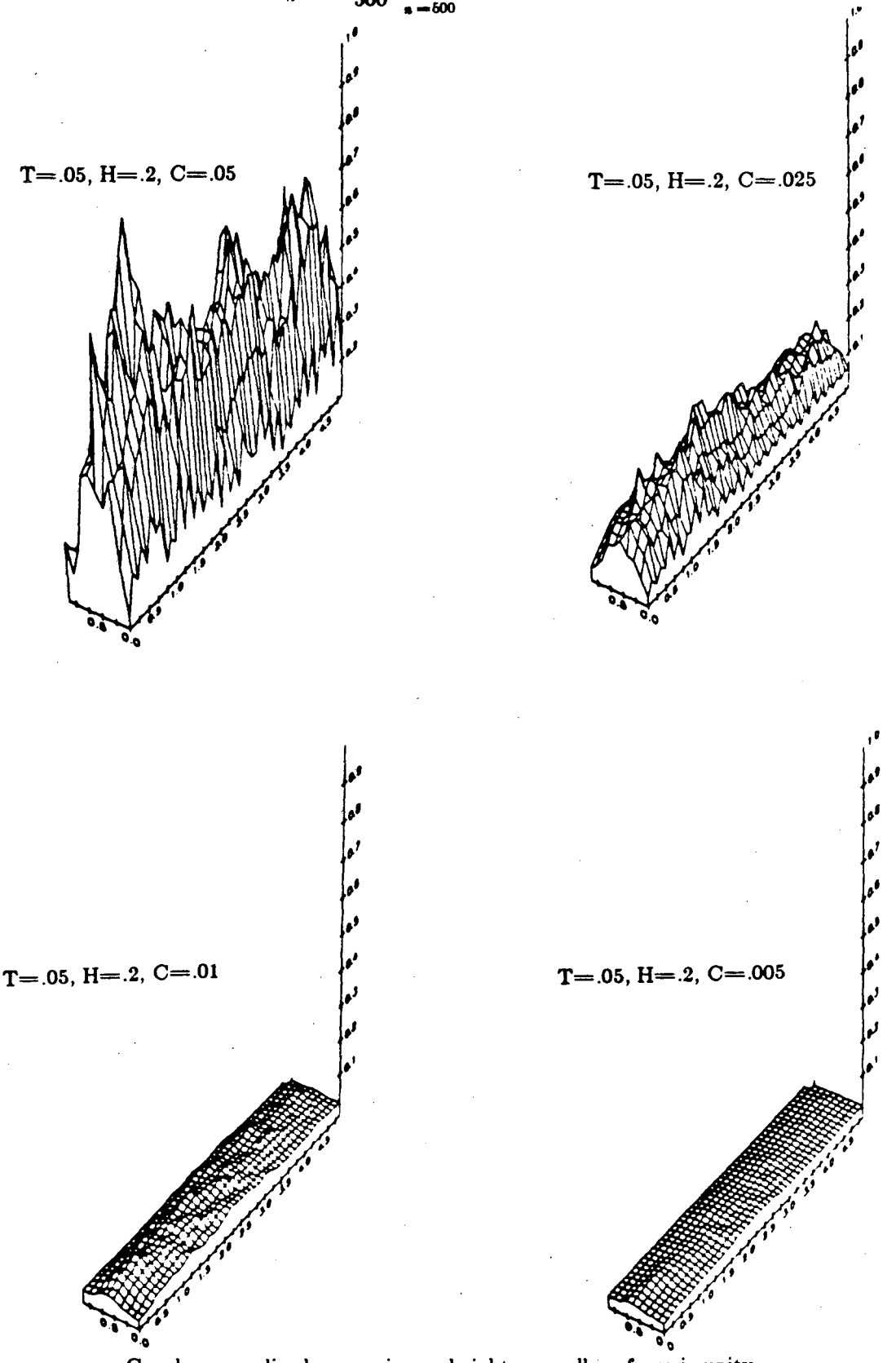

Graphs normalized so maximum height over all surfaces is unity.

FIGURE 21

DECAY OF TEMPORAL VARIANCE $Var_{i,j}$ FROM MEAN AT SELECT POINTS i, j IN DOMAIN

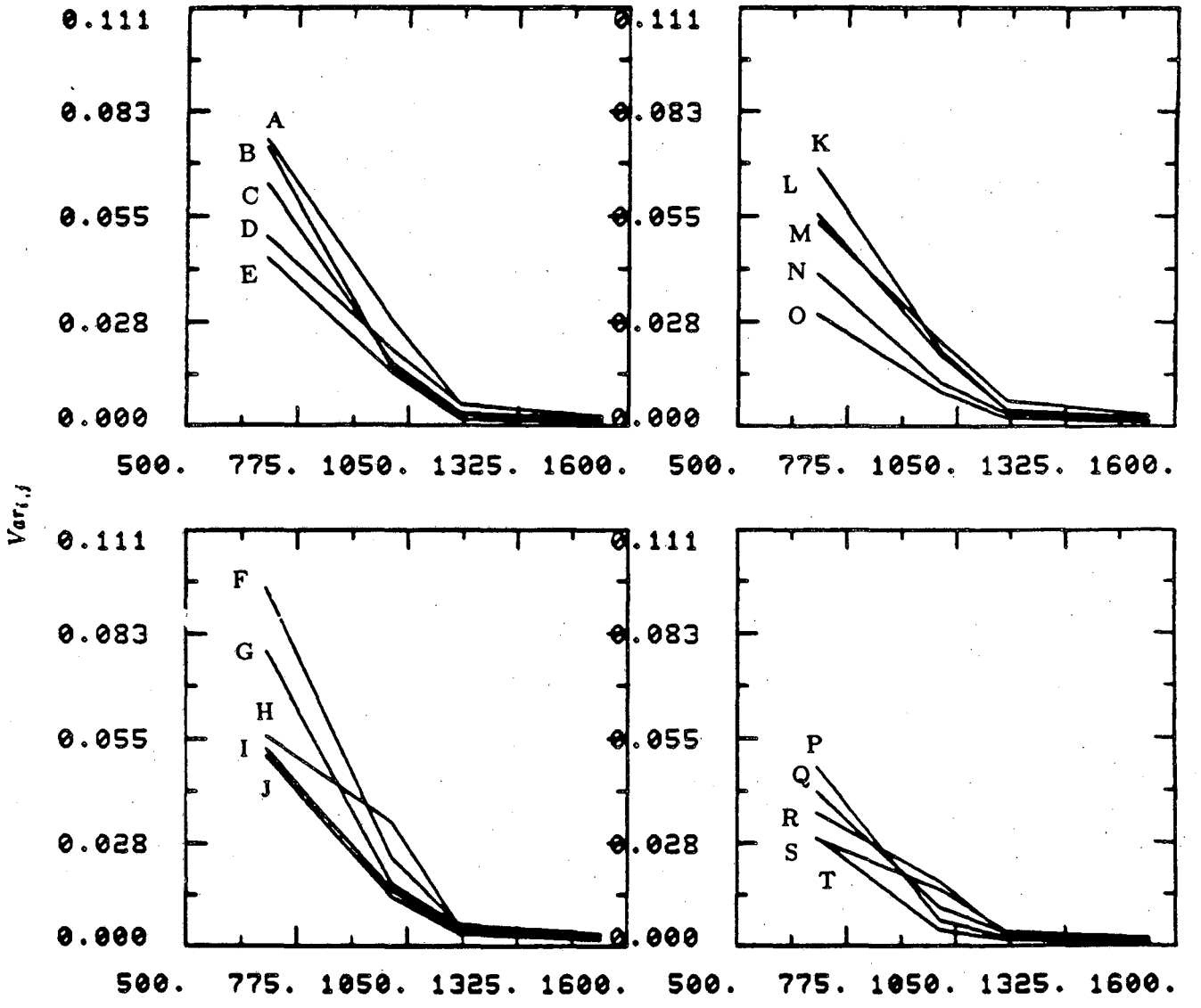

A=(1.,2.)
B=(2.,2.)
C=(3.,2.)
D=(4.,2.)
E=(5.,2.)
F=(1.,4.)
G=(2.,4.)
H=(3.,4.)
I=(4.,4.)
J=(5.,4.)

K=(1.,6.)
L=(2.,6.)
M=(3.,6.)
N=(4.,6.)
O=(5.,6.)
P=(1.,8.)
Q=(2.,8.)
R=(3.,8.)
S=(4.,8.)
T=(5.,8.)

FIGURE 22

CONVERGENCE OF MEAN VELOCITY FIELD FOR GIVEN NUMERICAL PARAMETERS TO MEAN OF FINEST (T=.05, H=.2, C=.005, WEND=5.) CALCULATION

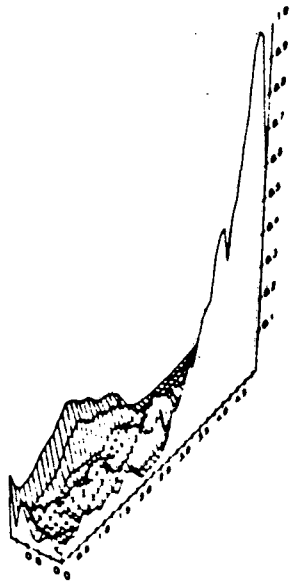

T=.05, H=.2, C=.05, WEND=5

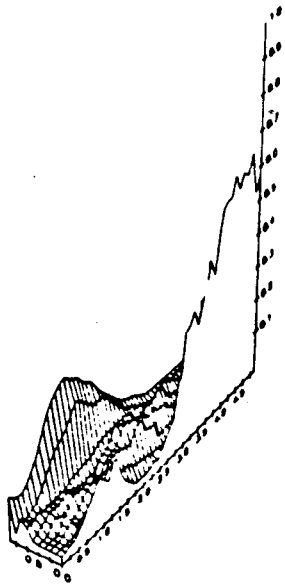

T=.05, H=.2, C=.025, WEND=5

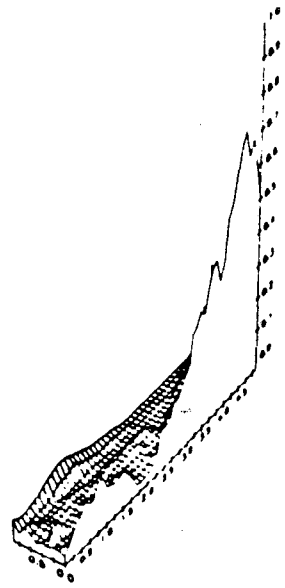

T=.05, H=.1, C=.025, WEND=5

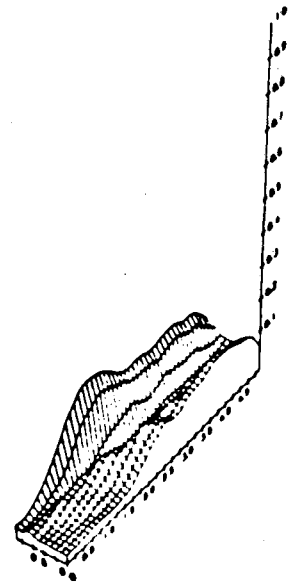

T=.05, H=.2, C=.01, WEND=5

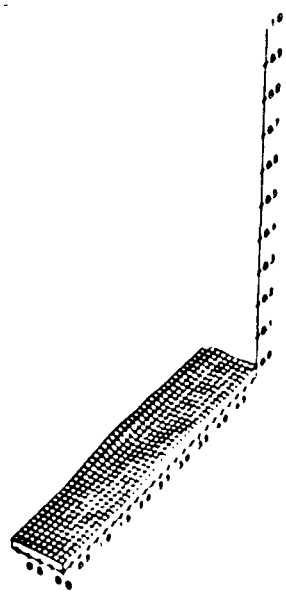

T=.05, H=.2, C=.005, WEND=10

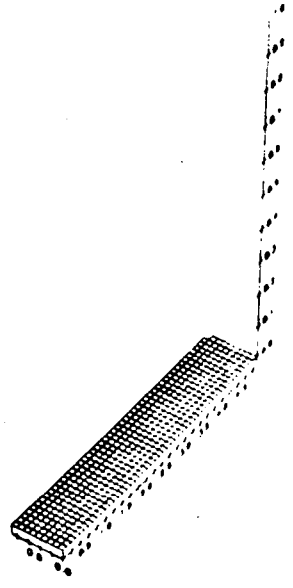

T=.05, H=.2, C=.005, WEND=5

Graphs normalized so maximum height over all surfaces is unity.

FIGURE 23

TEMPORAL VARIANCE $Err_{i,j}$ AGAINST FINEST MEAN $\bar{u}_{i,j}$ AS A FUNCTION OF SPACE

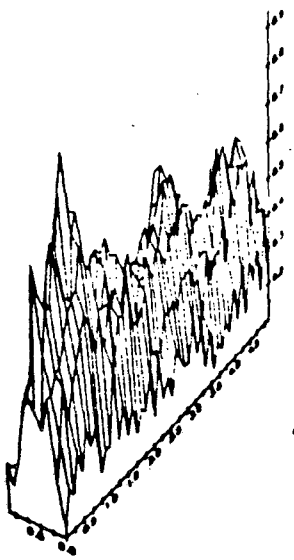

T=.05, H=.2, C=.05, WEND=5

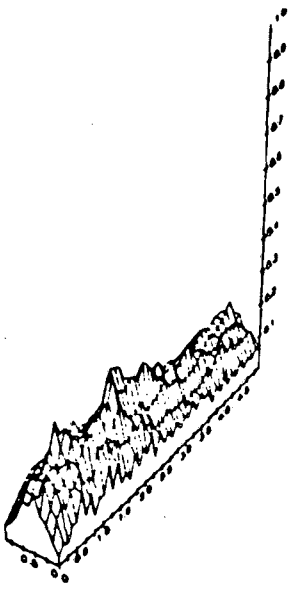

T=.05, H=.2, C=.025, WEND=5

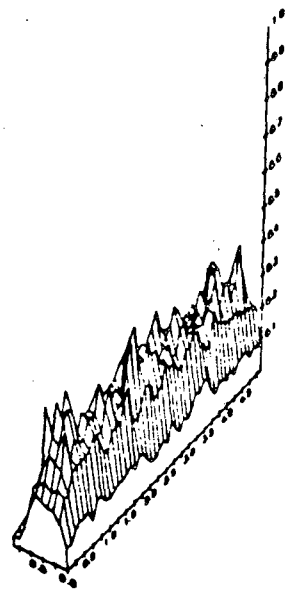

T=.05, H=.1, C=.025, WEND=5

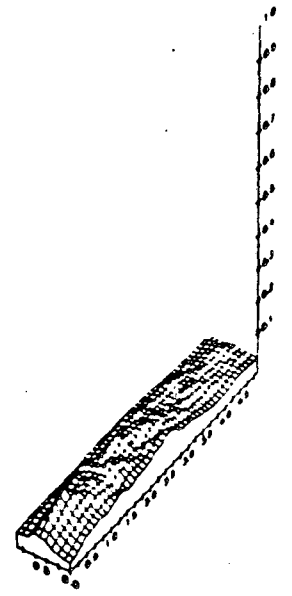

T=.05, H=.2, C=.01, WEND=5

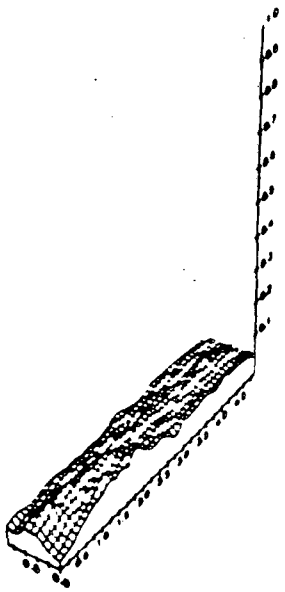

T=.025, H=.2,C=.01, WEND=5

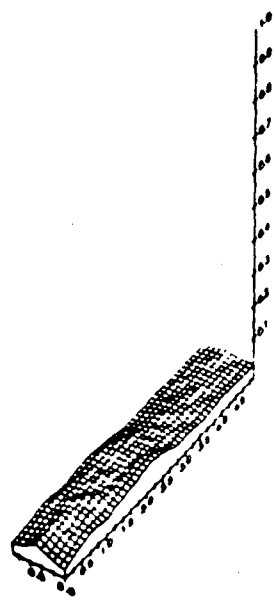

T=.05, H=.2, C=.005, WEND=10

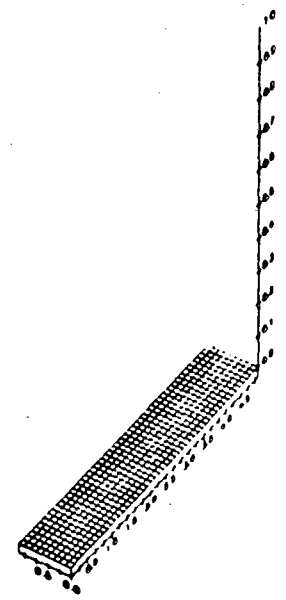

T=.05, H=.2, C=.005, WEND=5

FIGURE 24

REATTACHMENT POINT vs. TIME

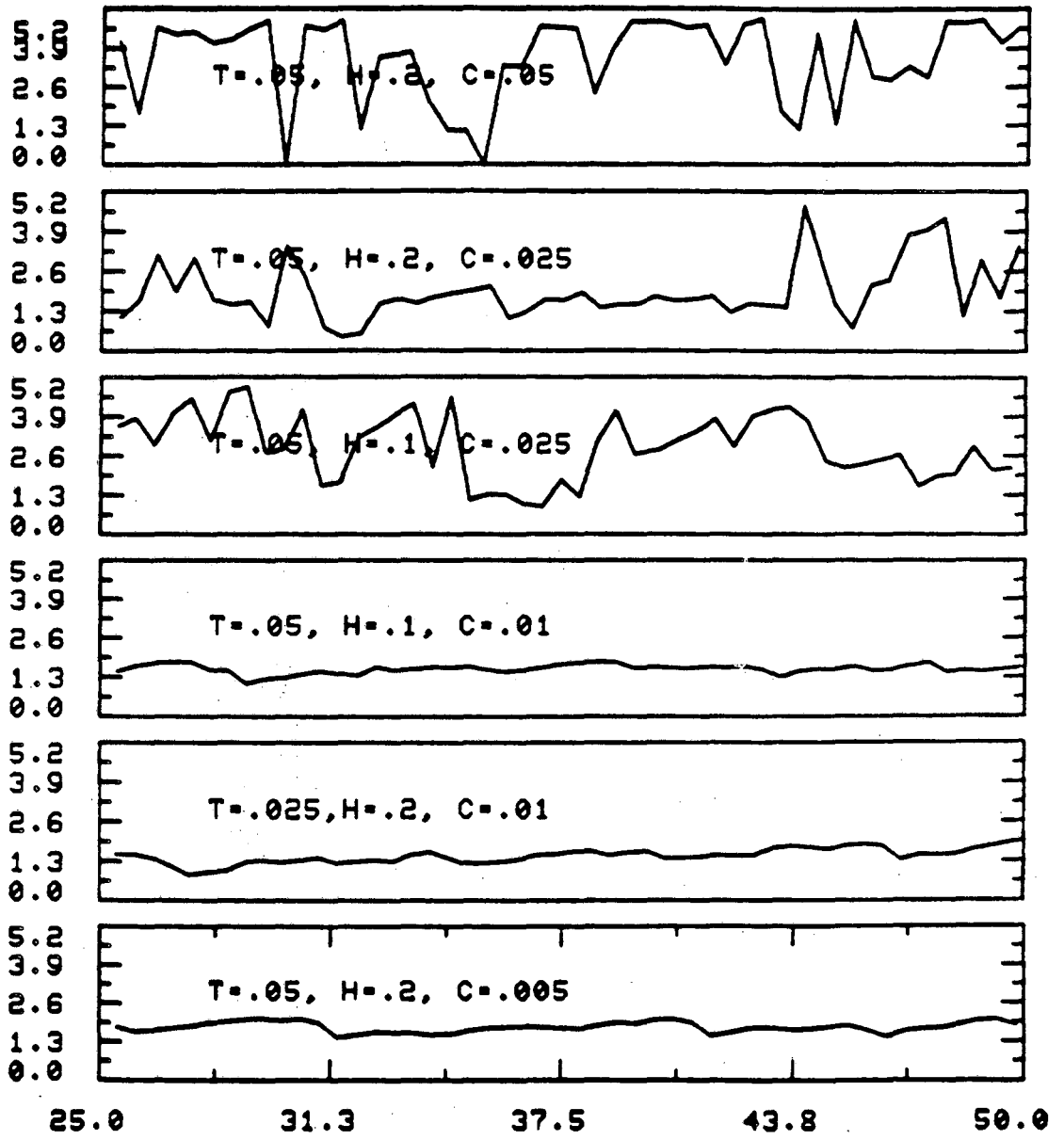

FIGURE 25

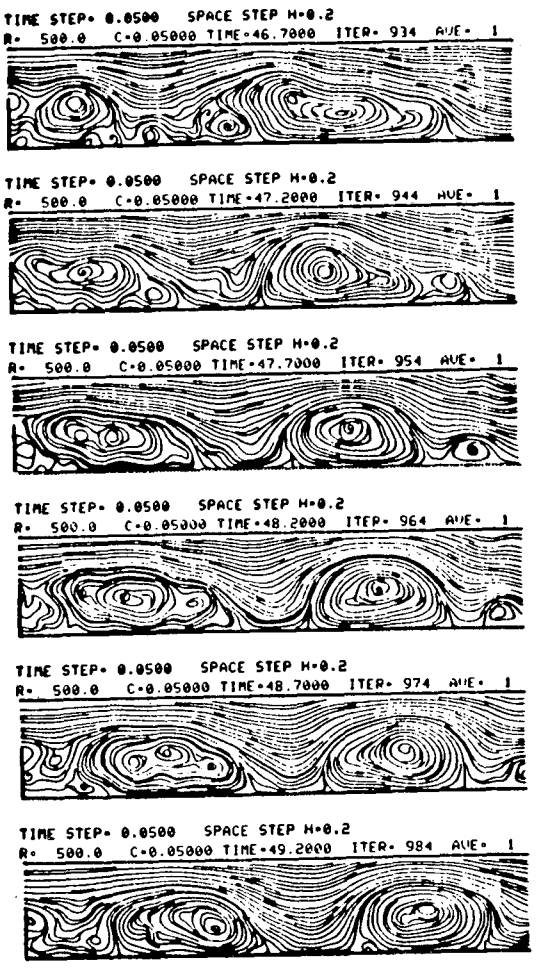

Figure 26a

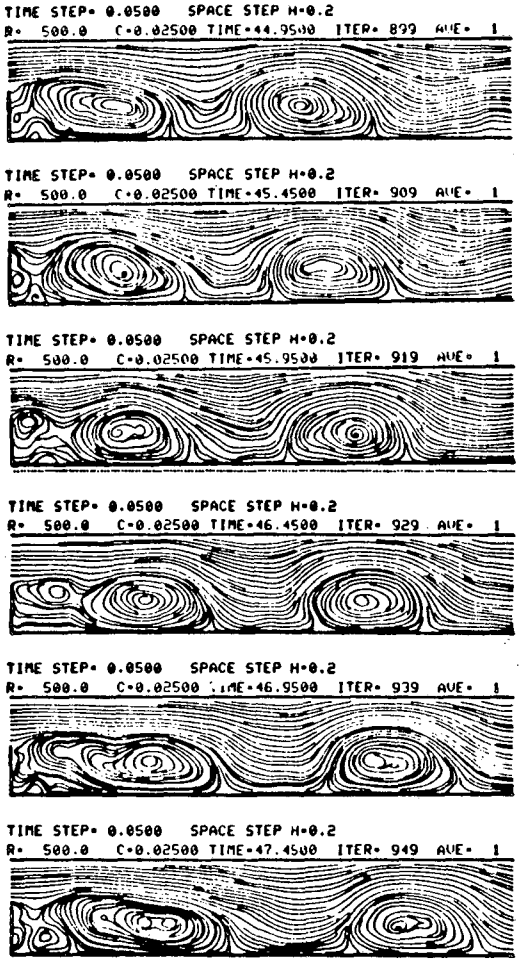

Figure 26b

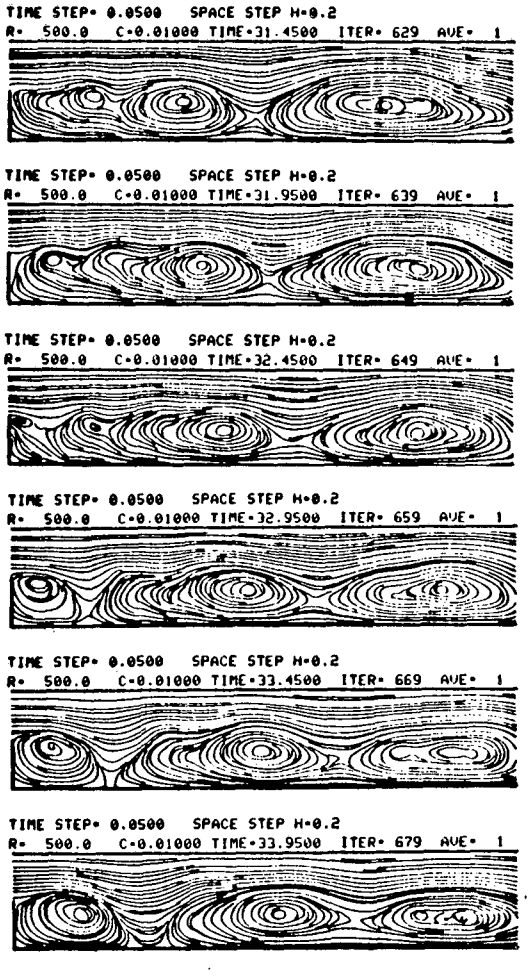

Figure 26c

$C = .05, .025, .01$, $H = .2$, $\Delta t = .05$, $W_{END} = 5$

FIGURE 26

FULLY DEVELOPED FLOW $R = 500$

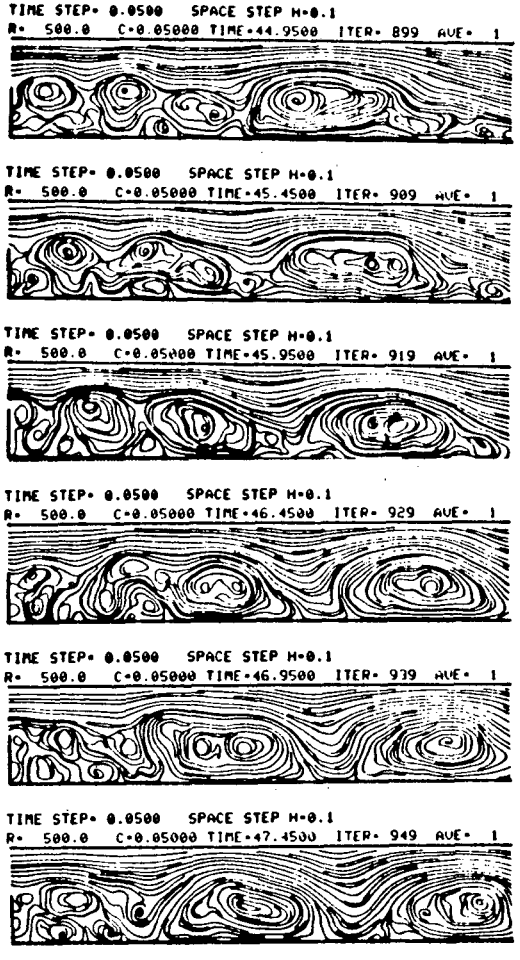

Figure 27a

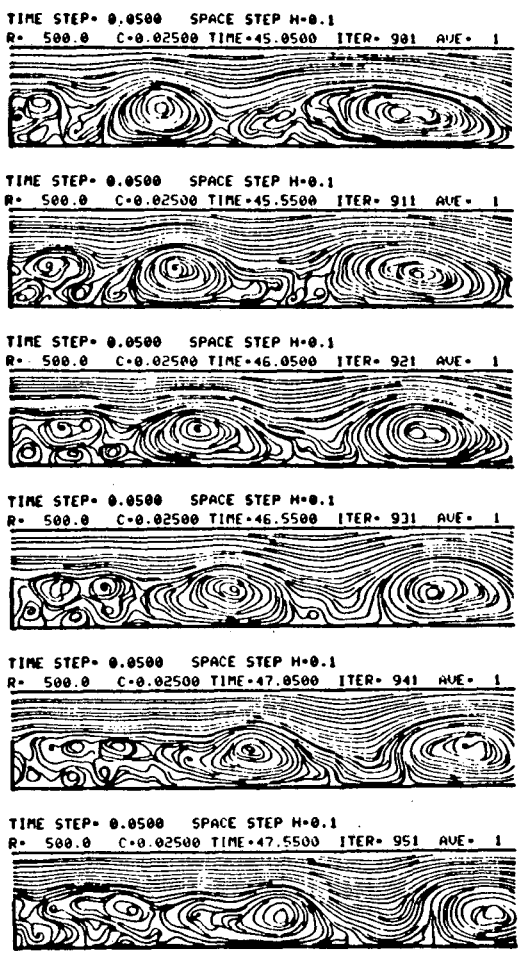

Figure 27b

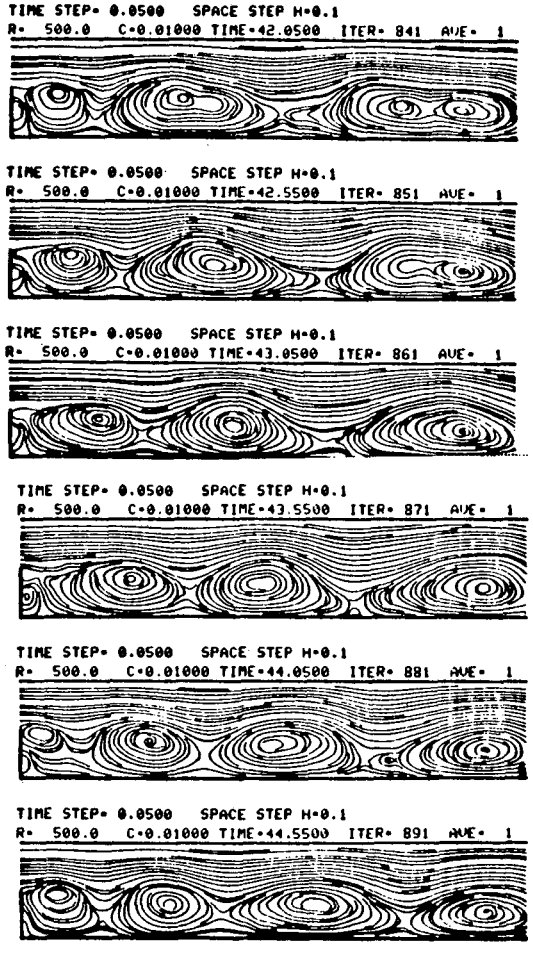

Figure 27c

$C = .05, .025, .01$, $H = .1$, $\Delta t = .05$, $W_{\text{END}} = 5$

FIGURE 27

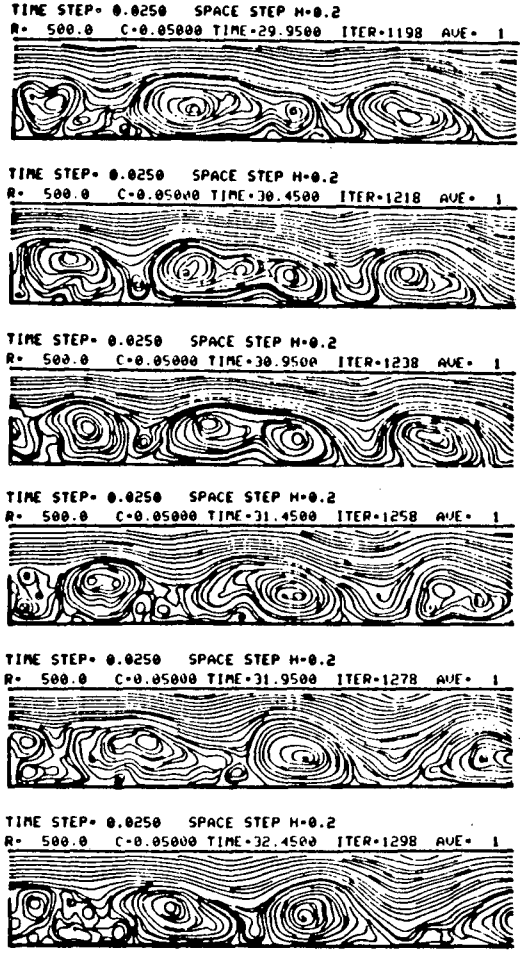

Figure 28a

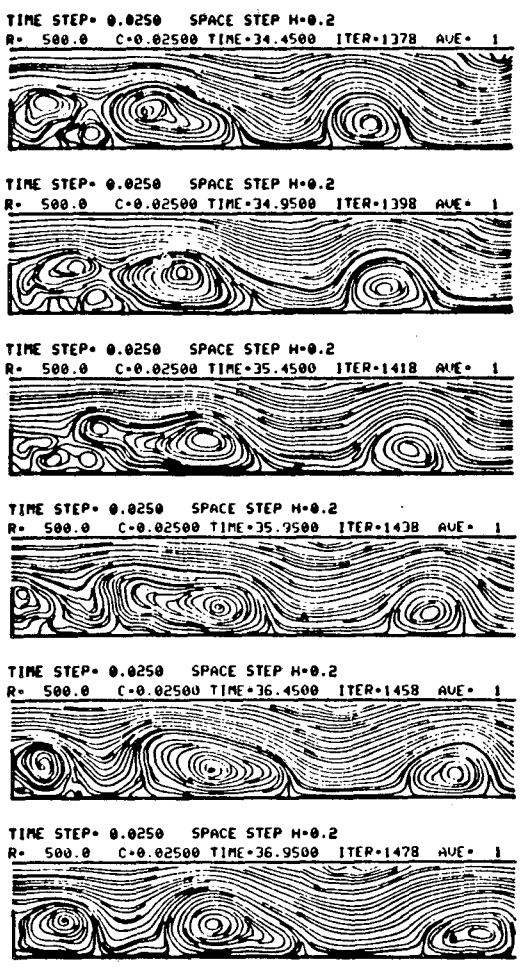

Figure 28b

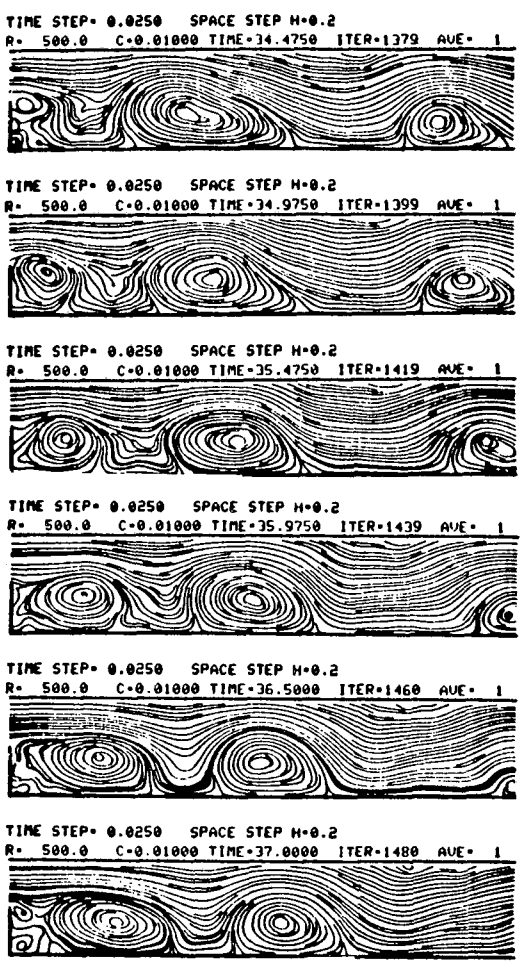

Figure 28c

$C = .05, .025, .01$, $H = .2$, $\Delta t = .025$, $W_{END} = 5$

FIGURE 28

FULLY DEVELOPED FLOW $R = 500$

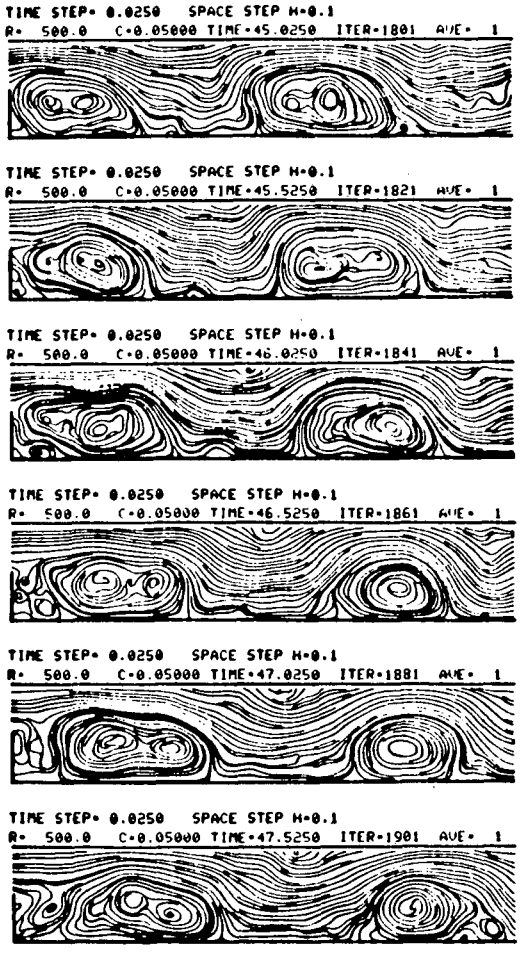

Figure 29a

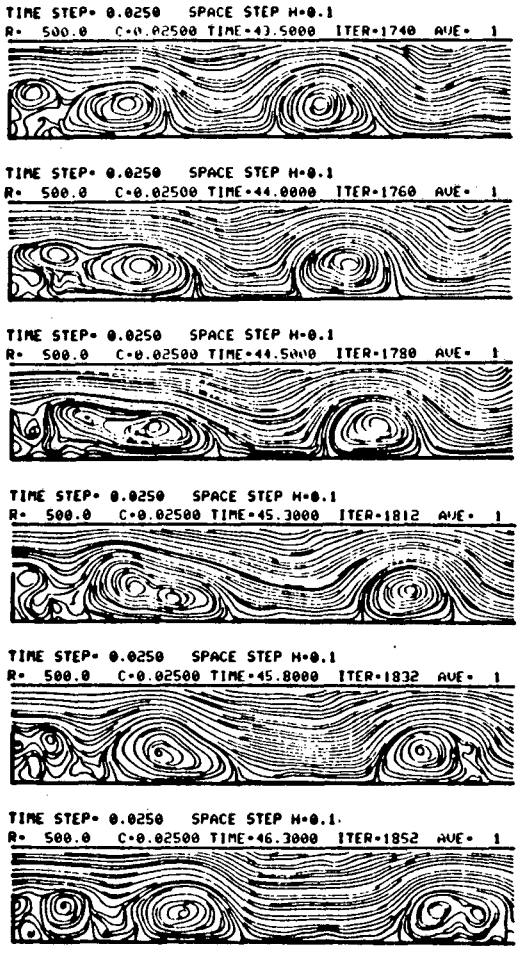

Figure 29b

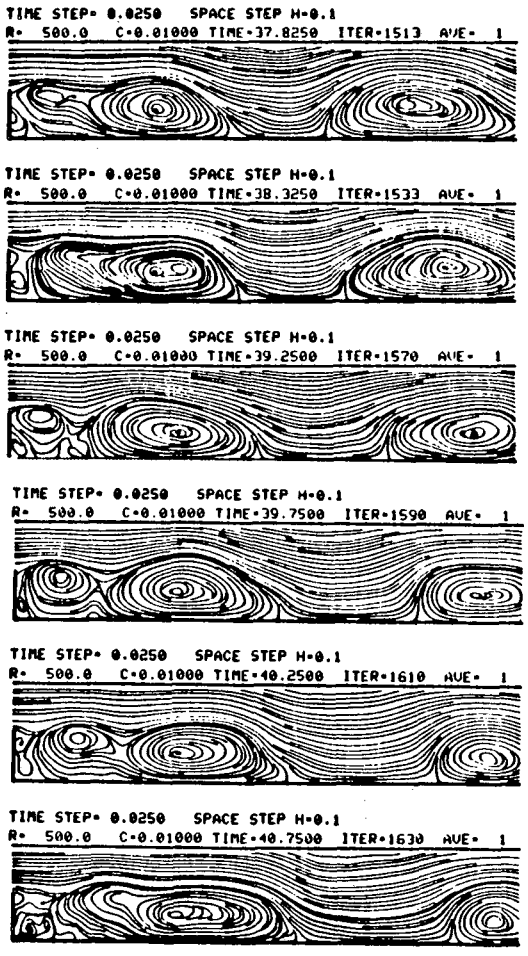

Figure 29c

$C = .05, .025, .01$, $H = .1$, $\Delta t = .025$, $W_{\text{END}} = 5$

FIGURE 29

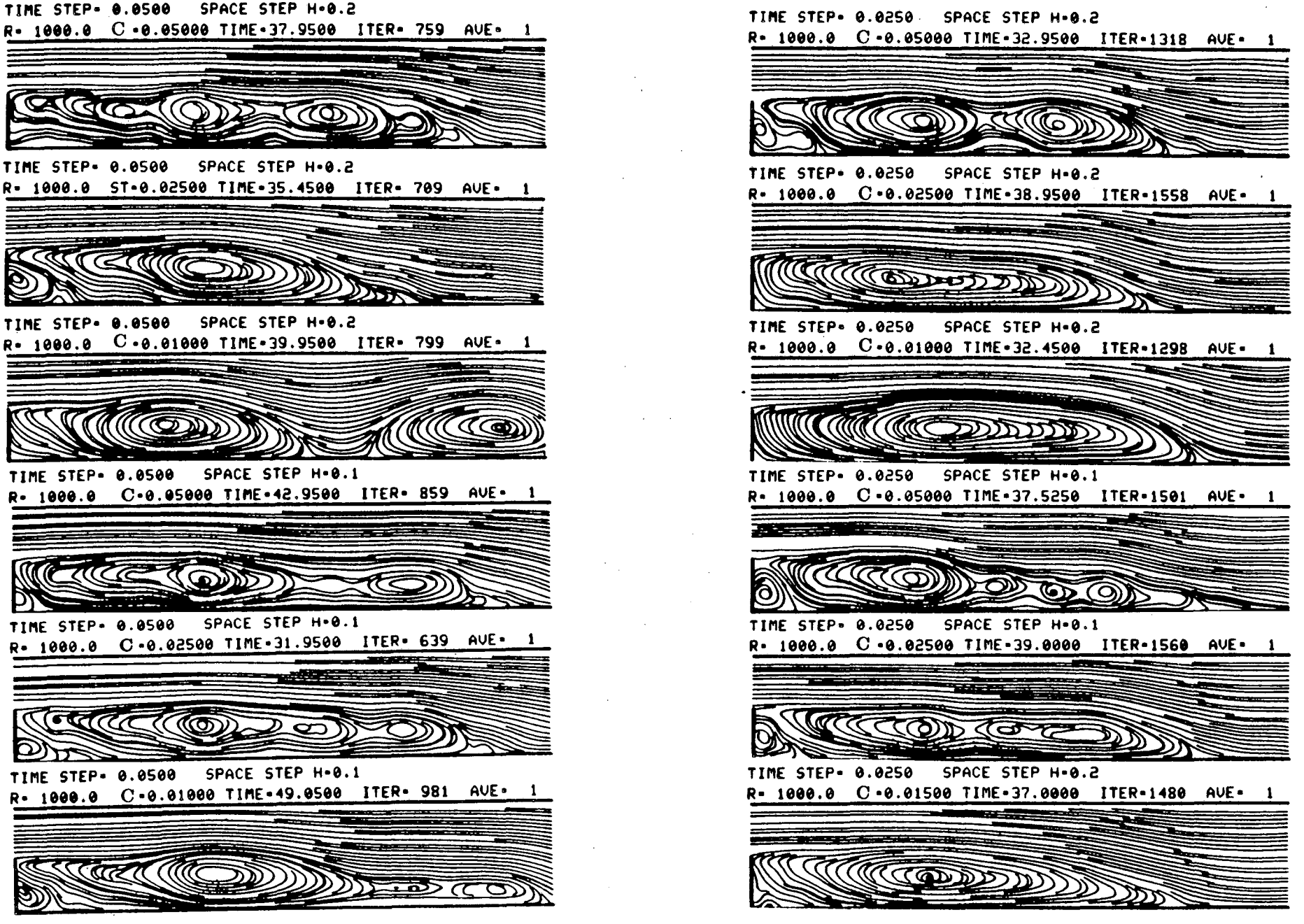

AVERAGE STREAMLINES OVER ONE SHEDDING CYCLE

FIGURE 28

LAWRENCE BERKELEY LABORATORY
TECHNICAL INFORMATION DEPARTMENT
UNIVERSITY OF CALIFORNIA
BERKELEY, CALIFORNIA 94720